

# The Limit of Photoreceptor Sensitivity: Molecular Mechanisms of Dark Noise in Retinal Cones

DAVID HOLCMAN and JUAN I. KORENBROT

Keck Center for Theoretical Neurobiology and Department of Physiology, School of Medicine, University of California at San Francisco, San Francisco, CA 94143

**ABSTRACT** Detection threshold in cone photoreceptors requires the simultaneous absorption of several photons because single photon photocurrent is small in amplitude and does not exceed intrinsic fluctuations in the outer segment dark current (dark noise). To understand the mechanisms that limit light sensitivity, we characterized the molecular origin of dark noise in intact, isolated bass single cones. Dark noise is caused by continuous fluctuations in the cytoplasmic concentrations of both cGMP and  $\text{Ca}^{2+}$  that arise from the activity in darkness of both guanylate cyclase (GC), the enzyme that synthesizes cGMP, and phosphodiesterase (PDE), the enzyme that hydrolyzes it. In cones loaded with high concentration  $\text{Ca}^{2+}$  buffering agents, we demonstrate that variation in cGMP levels arise from fluctuations in the mean PDE enzymatic activity. The rates of PDE activation and inactivation determine the quantitative characteristics of the dark noise power density spectrum. We developed a mathematical model based on the dynamics of PDE activity that accurately predicts this power spectrum. Analysis of the experimental data with the theoretical model allows us to determine the rates of PDE activation and deactivation in the intact photoreceptor. In fish cones, the mean lifetime of active PDE at room temperature is  $\sim 55$  ms. In nonmammalian rods, in contrast, active PDE lifetime is  $\sim 555$  ms. This remarkable difference helps explain why cones are noisier than rods and why cone photocurrents are smaller in peak amplitude and faster in time course than those in rods. Both these features make cones less light sensitive than rods.

**KEY WORDS:** phototransduction • phosphodiesterase • guanylate cyclase • cGMP • calcium

## INTRODUCTION

Rod photoreceptors reliably signal single absorbed photons (Baylor et al., 1979), but detection threshold is higher in cones. The limit of light detection varies among cones in different species, and even between cone subtypes in the same species (Miller and Korenbrot, 1993). Still, in complete darkness, even the most sensitive cones require the coincident absorption of several photons (some four to seven) to generate a detectable signal (Schnapf et al., 1990; Miller and Korenbrot, 1993; Donner et al., 1998). To be detected, light-dependent currents must exceed in amplitude intrinsic fluctuations of the photoreceptor dark membrane current referred to as “dark noise.” For example, in single cones of striped bass, the extrapolated single photon peak current amplitude is  $\sim 0.14$  pA (this report) and it is  $\sim 0.03$  pA in macaque cones (Schnapf et al., 1990). These signals are undetectable because they do not exceed the dark current noise variance,  $\sim 0.28$  pA<sup>2</sup> in bass and  $0.12$  pA<sup>2</sup> in macaque (0–20 Hz range) (Schnapf et al., 1990). In rods, in contrast, single photon peak photocurrent amplitude is  $\sim 1$  pA in toads (Baylor et al., 1979) and

$0.7$  pA in macaque (Baylor et al., 1984). These signals are readily detected above dark current noise of variance  $0.035$  pA<sup>2</sup> in toads (Baylor et al., 1980) and  $0.030$  pA<sup>2</sup> in macaque (0–20 Hz range) (Baylor et al., 1984).

To elucidate the molecular mechanisms underlying dark noise in cones and, hence, the limit of their sensitivity, we investigated the properties and molecular mechanisms of membrane current noise in dark-adapted, green-sensitive single cones of the striped bass. Cone dark noise has been previously characterized both as fluctuation in membrane voltage (Lamb and Simon, 1977; Schneeweis and Schnapf, 1999) and in membrane current (Schnapf et al., 1990; Rieke and Baylor, 2000; Sampath and Baylor, 2002). These studies have shown that dark noise consists of light-sensitive and -insensitive components. The light-sensitive component originates from two principal molecular sources: (1) occasional, spontaneous thermal activation of visual pigment (VP) molecules and (2) continuous fluctuations in the cytoplasmic concentration of cGMP and  $\text{Ca}^{2+}$ , as well as in the activity of cGMP-gated (CNG) ion channels. The two components are readily distinguished from each other because of their distinct kinetics: noise that originates from VP excitation has a time course identical

Correspondence to Juan I. Korenbrot: [juan@itsa.ucsf.edu](mailto:juan@itsa.ucsf.edu)

D. Holcman's permanent address is Department of Mathematics and Computer Science, Weizmann Institute of Science, Rehovot 76100, Israel.

*Abbreviations used in this paper:* GC, guanylate cyclase; CNG, cGMP-gated; PDE, phosphodiesterase; VP, visual pigment.

to that of the dim light photocurrent, whereas the continuous noise does not (Rieke and Baylor, 2000).

In an elegant study in toad rods, Rieke and Baylor (1996) demonstrated that the continuous component of dark noise consists of components of distinct frequency. High frequency noise is generated by open to close transitions in the CNG ion channels, while low frequency noise is caused by fluctuating cGMP concentration due to variance in phosphodiesterase (PDE) activity. This enzyme catalyzes cGMP hydrolysis and its activation by excited rhodopsin is at the core of the biochemical mechanisms of phototransduction (for reviews see Pugh and Lamb, 2000; Ebrey and Koutalos, 2001). In an extension of their studies to cone photoreceptors in tiger salamander retina, Rieke and Baylor (2000) found that dark noise characteristics differ among cones depending on their VP. In all cone subtypes, noise lacks discrete, single photon transitions. In tiger salamander retina, the continuous dark noise in red-sensitive, L cones arises from spontaneous VP excitation that occurs at a rate of  $\sim 1,000 \text{ s}^{-1}$  at  $20^\circ\text{C}$  (Sam-path and Baylor, 2002), much higher than that of rhodopsin in tiger salamander rods ( $\sim 0.03 \text{ s}^{-1}$  at  $20^\circ\text{C}$ ) (Vu et al., 1997). In blue-sensitive S cones, on the other hand, dark noise does not appear to arise from VP thermal excitation because its time characteristics differ from those of the dim light photoresponse (Rieke and Baylor, 2000). In cones of other species studied to date (turtle, Lamb and Simon, 1977; macaque, Schneeweis and Schnapf, 1999; and fish, this report), dark current noise does not appear to arise from thermal VP excitation since its power spectrum is different from that of the dim light photoresponse.

We present experimental data to identify the molecular origin of the continuous component of dark noise in green sensitive single cones of the bass retina. We demonstrate that dark noise is not caused by high rate spontaneous visual pigment excitation, but rather by fluctuations in cytoplasmic levels of cGMP and  $\text{Ca}^{2+}$  in darkness. Furthermore, in the absence of  $\text{Ca}^{2+}$  fluctuations, cGMP fluctuations are caused by spontaneous, thermal activation of PDE. This is the same mechanism known to cause the continuous dark noise in rods (Rieke and Baylor, 1996) and which had been suggested as a source of noise in blue sensitive cones (Rieke and Baylor, 2000).

Mathematical analysis of the features of dark noise allows us to characterize for the first time the kinetics of PDE activation in an intact, functional cone. The time course of the dim light photocurrent is faster in cones than in rods in all species studied to date (for reviews see Korenbrot, 1995; Pugh and Lamb, 2000; Ebrey and Koutalos, 2001). Detailed quantitative models suggest that this acceleration can reflect any one, or any combination, of three principal kinetic events: (1) the rate of

deactivation of excited visual pigment, (2) the rate of inactivation of PDE, and (3) the rate of activation of guanylate cyclase (GC) (Sneyd and Tranchina, 1989; Ichikawa, 1994; Hamer and Tyler, 1995; Korenbrot and Rebrink, 2002). With respect to PDE, biochemical studies have demonstrated that the catalytic efficiency of active PDE is essentially the same in rods and cones (Gillespie and Beavo, 1988; Cote et al., 2002). In contrast, our analysis of dark noise indicates that the lifetime of the active state of PDE is  $\sim 10$  times shorter in cones than in rods. This remarkable difference not only helps explain why cones are noisier than rods, but also why cone photocurrents are smaller in peak amplitude and faster in time to peak than those in rods. The limitations of a small signal superimposed on high noise makes the cone less sensitive to light than the rod.

## MATERIALS AND METHODS

### Materials

Striped bass were received from a commercial supplier (Professional Aquaculture Services), maintained in an aquaculture facility under 14:10 L:D cycles and fed ad lib. Fish were dark adapted for 40 min and killed following procedures approved by the IACU committee at University of California at San Francisco (UCSF). In complete darkness and with the aid of IR-sensitive TV cameras and viewers, we obtained a suspension of cone photoreceptors in Ringer's solution by mechanical trituration of isolated retinas first subjected to gentle proteolysis (collagenase and hyaluronidase), as described in detail elsewhere (Miller and Korenbrot, 1993). Zaprinast, 8-p-chlorophenylthio-cGMP (8-cpt-cGMP), and nifedipine were obtained from Calbiochem.

### Electrical Recording

Isolated cone photoreceptors were firmly attached to a concanavilin-A-coated glass coverslip that formed the bottom of an open electrophysiological recording chamber. The chamber was held on an inverted microscope equipped with DIC contrast enhancement, and the cell-bathing solution was intermittently exchanged. Microscopic observations were conducted under IR illumination (840–880 nm) with the aid of video cameras and monitors. Composition of the cell-bathing Ringer's solution was (in mM) NaCl (126), CsCl (10), KCl (2.4),  $\text{NaHCO}_3$  (5),  $\text{NaH}_2\text{PO}_4$  (1),  $\text{MgCl}_2$  (1),  $\text{CaCl}_2$  (1), nifedipine (0.01), minimum essential medium amino acids and vitamins (GIBCO-BRL), glucose (10), BSA (0.1 mg/ml), and HEPES (10). pH was 7.5 and osmotic pressure 310 mOsm.

We measured membrane current at room temperature under voltage clamp using tight-seal electrodes in the whole-cell mode. Electrodes were produced from aluminosilicate glass (Corning 1724,  $1.5 \times 1.0 \text{ mm od} \times \text{id}$ ). Currents were recorded with a patch clamp amplifier (Axopatch 1D; Axon Instruments). The analogue signal was simultaneously low pass filtered (0–100 Hz) through two different 8 pole filters, one a Bessel filter and the other a Butterworth filter (Frequency Devices) and then digitized on line at 300 Hz (Digidata1322A and pClamp software; Axon Instruments).

The composition of the normal tight-seal electrode-filling solution was (in mM)  $\text{K}^+$  gluconate (115),  $\text{K}^+$  aspartate (20), KCl (33),  $\text{MgCl}_2$  (1 free), GTP (1), ATP (3), and MOPS (10). pH was

7.25 and osmotic pressure 305 mOsM. For different experimental purposes, the electrode-filling solution was modified to yield one of three conditions. (1) Ca<sup>2+</sup>-buffered solution contained normal GTP, ATP, and in addition 10 mM BAPTA titrated with CaCl<sub>2</sub> to yield 400 nM free Ca<sup>2+</sup> (confirmed using BAPTA absorption spectra as a Ca<sup>2+</sup> indicator). Ca<sup>2+</sup> buffers were designed using WinMaxC software ([www.stanford.edu/~cpatton](http://www.stanford.edu/~cpatton)). (2) Nucleotide-free solution lacked ATP and GTP, either in a normal or a Ca<sup>2+</sup>-buffered formulation. (3) Triphosphate nucleotide-free, Ca<sup>2+</sup>-buffered solution containing added cyclic nucleotides.

Light stimuli were delivered with an epiillumination system that used the microscope objective as its final lens (Nikon Fluor 40×/1.3 NA oil). The focused image of an adjustable aperture placed on the optical path limited illumination to a 40 μm diameter circle centered on the cell under study. Light was generated by a DC operated Tungsten source. Narrow band interference (10 nm bandwidth) and calibrated neutral density filters controlled color and intensity, while stimulus duration was controlled with an electronically triggered fast electromechanical shutter (Vincent and Associates, Rochester, NY). Light intensity was measured with a calibrated photodiode placed on the microscope stage at the same position as the cells (UDT Sensors).

### Single Cell Superfusion

The tip of a polyimide-coated silica capillary (PT Technologies) 125 μm ID was placed within ~100 μm from the cell under study and in the same vertical plane. Solution flowed through the superfusing capillary under positive pressure (~50 mm Hg). Flow was controlled with an electronically triggered pinch valve (BPS-4; ALA Scientific). Upon activation of the valve, solution change around the cell was complete within ~50 ms.

### Hydroxylamine Treatment

A dark-adapted single cone was first positioned in the optical center of the imaging lens and then superfused with the single cell system described above. Superfusing solution consisted of (in mM) hydroxylamineHCl (60), NaCl (63), CsCl (5), KCl (1.2), NaHCO<sub>3</sub> (2.5), NaH<sub>2</sub>PO<sub>4</sub> (0.5), MgCl<sub>2</sub> (1), CaCl<sub>2</sub> (1), and HEPES (20). pH was 7.5 and osmotic pressure 310 mOsM. The selected cone was superfused for exactly 120 s and then washed by continuous bath perfusion with normal Ringer's for ~5 min. Tight seal electrodes were applied to the treated cone only after this extensive washout. Thus, hydroxylamine was absent from the cell at the time of electrophysiological measurements.

### Data Analysis

Power spectral density of steady currents processed through a Butterworth filter (0–100 Hz) were computed from 13.66-s-long data episodes sampled at 300 Hz (4,098 points per episode) (Clampfit; Axon Instruments). In some datasets, there was a small, but detectable, linear drift over the sampling period; when such drift was apparent, it was removed by subtracting the mean slope of the drift before computing power spectra. To reduce the dataset, each individual power spectrum was processed by computing a box car average over one to three data points between 0 and 10 Hz, five data points between 10 and 40 Hz, 10 data points between 40 and 90 Hz, and 16 data points between 90 and 150 Hz. In data presentation, the mean of the box car average is indicated as a symbol and its standard deviation as an error bar. For graphic convenience, only the positive error bars are drawn in the illustrations. Experimental data were fit with defined mathematical expressions using nonlinear least square minimization algorithms (Origin; Origin Labs). In text and tables, the reported statistical errors are standard deviations.

To determine the power in the current noise (variance) over a specified bandwidth (typically 0–20 Hz), nonaveraged power spectra were integrated and the value of the integral at 20 Hz measured. Light-sensitive noise was computed from the difference in variance of the current measured in complete darkness and that measured in the same cell in the continuous presence of light at intensities that saturated the photocurrent amplitude (typically  $1.2 \times 10^5$  540 nm photons/μm<sup>2</sup> sec). Numerical solutions of systems of simultaneous differential equations were computed using 20Sim modeling software (ControlLab Products B.V.).

## RESULTS

There are two types of cone photoreceptors in the retina of striped bass, single and twins. The VP peak absorbance is 540 nm in single cones and 620 nm in each member of a twin pair (Miller and Korenbrot, 1993). In complete darkness, the voltage-clamped holding current in isolated single cones fluctuates in amplitude about a mean value (Fig. 1). This current noise arises from statistical variance in the activity of light-sensitive, CNG ion channel in the cell's outer segment, as well as in the activity of voltage-gated channels in the inner segment. To characterize the light-sensitive component of dark noise at –40 mV, we measured fluctuations in the holding current of cones bathed in a Ringer's solution containing 100 μm nifedipine and 10 mM Cs<sup>+</sup>. These chemicals effectively block L-type Ca<sup>2+</sup> and Kir channels, the most active voltage-gated channels in cones at –40 mV in bass cones (unpublished data), as they do in cones of other species (Barnes and Hille, 1989; Maricq and Korenbrot, 1990a,b). We conducted experiments at –40 mV holding voltage because this is near the resting voltage in intact, dark-adapted cones.

We thought it important to demonstrate that phototransduction is unaffected by the added channel blockers. In Fig. 1 B, we illustrate typical photocurrents measured at –40 mV holding voltage in a single cone in the presence of extracellular Cs<sup>+</sup> and nifedipine. The waveform, time to peak, and light sensitivity of these currents are indistinguishable from those recorded absent the blockers (Miller and Korenbrot, 1993). For a 10-ms flash stimulus, the peak photocurrent amplitude increases with light intensity as described by the Michaelis-Menten equation

$$I = \frac{I_{max}E}{E + \sigma}, \quad (1.1)$$

where  $I_{max}$  is the maximum current amplitude,  $E$  is light intensity, and  $\sigma$  is the intensity at half-maximum amplitude. For 11 different cones, we found mean  $I_{max} = 24.9 \pm 4.6$  pA and  $\sigma = 168.6 \pm 60$  photons/μm<sup>2</sup>. Given a calculated cross section of absorption of 1.92 μm<sup>2</sup> for the bass cone outer segment,  $\sigma = 319 \pm 114$  photoisomerizations. Amplitude of the bass cone single photon response, extrapolated from responses in the linear range, is ~0.14 pA.

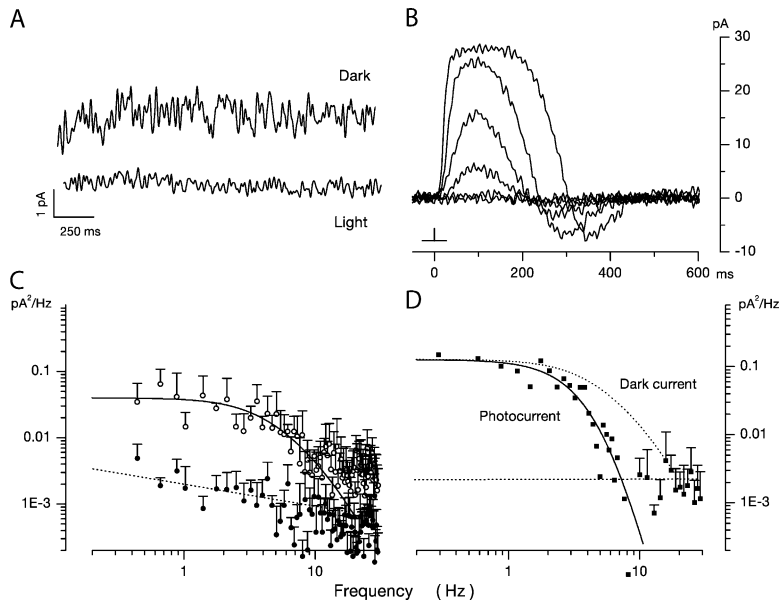


FIGURE 1. Dark noise and photocurrents in bass single cone at room temperature. Membrane current measured under voltage clamp at  $-40$  mV holding voltage. (A) Membrane current in the dark (top trace) and under continuous illumination ( $1.2 \times 10^5$  540 nm photons/ $\mu\text{m}^2$  s) (bandpass 0–40 Hz). The mean holding current in dark was 9.7 pA and noise variance  $0.21 \text{ pA}^2$ . The mean holding current in light was 28.9 pA and noise variance  $0.02 \text{ pA}^2$ . (B) Photocurrent activated by 10-ms flash of 540-nm light presented at time zero. Responses generated by flashes that delivered 2.3, 10.8, 62, 246, 1,486, and 6,795 photons/ $\mu\text{m}^2$ . The light dependence of the photocurrent peak amplitude reached half maximum amplitude at  $\sigma = 220$  photons/ $\mu\text{m}^2$  (Eq. 1.1). (C) Power spectra of the fluctuations in current amplitude in darkness (open symbols) and under continuous illumination (filled symbols) shown in A. The continuous line over the data is a best fit theoretical function detailed in the text (Eq. 1.13). The dashed line over the data in light is a straight line optimally fit to the data points. (D) Power spectrum of the photocurrent generated by the 62 photon/ $\mu\text{m}^2$  photon flash shown in B. The continuous line over

the data is an optimally fit product of four identical Lorentzians (Eq. 1.2) with  $\alpha = 5.04$  Hz. The dotted line is the function that describes dark current noise spectrum (from C) shifted to match the zero frequency asymptote. It is drawn to illustrate the difference between photocurrent and dark current noise spectra.

#### Dark Current Noise in Normal Bass Single Cones

Typical holding currents measured in the 0–40 Hz frequency range using a Butterworth filter are illustrated in Fig. 1 A. Shown are currents measured in the same cell in darkness and under continuous illumination sufficient to saturate the photocurrent. For nine cells, the mean dark holding current was  $-4.2 \pm 10.1$  pA and fluctuations about the mean had an average variance of  $0.28 \pm 0.15 \text{ pA}^2$  (0–20 Hz). For the same cells in the light, the mean holding current was  $15.2 \pm 9.5$  pA, and the noise average variance was  $0.02 \pm 0.01 \text{ pA}^2$  (0–20 Hz). Variance of the light-sensitive component then was  $0.258 \pm 0.13$ . Power spectral-density analysis of the current fluctuations allows additional quantitative characterization of dark–light noise difference. At frequencies  $< \sim 30$  Hz, power density in dark current noise increased with frequency along a function illustrated as the continuous line over the data points in Fig. 1 C. The function is discussed below in the theoretical section. Over the same frequency, the power density in the light was not only much smaller in amplitude, but increased inversely with frequency with a relatively shallow slope (Fig. 1 C). At frequencies  $> \sim 30$  Hz (and up to the limit of our sampling at 100 Hz), dark and light noises were practically indistinguishable from each other and essentially independent of frequency. Henceforth, we use “dark noise” to mean specifically the difference noise between dark and light currents. Because light-sensitive CNG ion channels are exclusively localized in the outer segment “dark current noise” is synonymous with “outer segment current noise.”

In rod photoreceptors, spontaneous thermal rhodopsin activation gives rise to discrete, large transients in the dark current. The time course of these shot events (and the corresponding frequency power spectrum) is identical to that of the dim light photocurrent in the same cell (Yau et al., 1979; Baylor et al., 1980). In bass single cones, we did not observe discrete shot events in the dark current. To analyze the origin of dark current fluctuations, we compared the power spectra  $S(\omega)$  (power spectral-density function) of the dark noise current (Fig. 1 C) and the dim flash photocurrent (Fig. 1 D). The photocurrent power spectrum is well fit by the product of four Lorentzians of identical rate (continuous line in Fig. 1 D).

$$S(\omega) = S(0) \prod_{n=1}^4 \left[ \frac{1}{\omega^2 + \alpha^2} \right], \quad (1.2)$$

where  $S(0)$  is the zero frequency variance. This function has been used before to describe the photoreponse of both rods and cones in the frequency domain (Lamb and Simon, 1977; Baylor et al., 1980; Schnapf et al., 1990). It does not represent a specific molecular mechanism; it is a useful descriptive equation. Data of quality similar to that in Fig. 1 were collected in 11 different cells and the mean value of  $\alpha$  was  $5.72 \pm 0.79$  Hz. Expression 1.2 with  $\alpha = 5.72$  does not fit the power spectra of the dark noise (Fig. 1 C). Our finding in bass single cones is similar to previous results of dark noise analysis in cones of other species (Lamb and Simon, 1977; Schnapf et al., 1990; Schneeweis and

Schnapf, 1999). This fact reveals that individual fluctuations whose sum is the observed dark noise have a time course different than that of the dim light photocurrent.

In rods, the power spectra of the discrete components of dark noise and the dim light photocurrent are essentially identical; a finding that indicates that spontaneous VP excitation is the cause of the discrete dark noise (Baylor et al., 1984; Vu et al., 1997). The same finding is true in L-type salamander cones (Rieke and Baylor 2000; Sampath and Baylor 2002) and transgenic rods expressing human red-sensitive cone VP (Kefalov et al., 2003). The dissimilarity between the power spectra of dark noise and of dim light photocurrents indicates that thermal VP excitation is not the dominant molecular source of dark noise in bass single cones. Experimental affirmation of this conclusion is presented below.

#### *Dark Current Noise in Ca<sup>2+</sup>-buffered Cones*

The light-sensitive current in cone photoreceptors is sustained by flux through CNG ion channels in the outer segment membrane. Light-sensitive current fluctuations, hence, must arise either from open-to-close transitions in the active CNG channels or from fluctuations in the cytoplasmic levels of cGMP. Current fluctuations due to channel flicker have been characterized in membrane patches detached from bass cone outer segments (Picones and Korenbrot, 1994). In the 0–1,000 Hz frequency range, the power spectrum of these fluctuations is well described by the sum of two Lorentzians of characteristic frequencies  $f_1$  and  $f_2$ .  $f_1 = 26$  Hz reflects the kinetics of cGMP binding to the channels.  $f_2 = 318$  Hz reflects channel flickering kinetics. Because channel flicker is fast, it does not contribute to dark noise in the frequency domain explored in this report, 0–30 Hz.

In cones photoreceptors, cGMP fluctuations can arise indirectly from fluctuations in cytoplasmic Ca<sup>2+</sup>. Ca<sup>2+</sup> regulates both the activity of guanylate cyclase (GC) (Koch and Stryer, 1988; Gorczyca et al., 1995), the enzyme that synthesizes cGMP, and the ligand sensitivity of CNG channels (Rebrik and Korenbrot, 1998; Korenbrot and Rebrik, 2002). To distinguish the effects of fluctuations in cGMP from fluctuations in cytoplasmic Ca<sup>2+</sup>, we measured current in cells in which potential cytoplasmic Ca<sup>2+</sup> fluctuations were attenuated by loading their cytoplasm with 10 mM BAPTA titrated to yield 400 nM free Ca<sup>2+</sup>, the free Ca<sup>2+</sup> concentration measured in dark-adapted cones of the tiger salamander (Sampath et al., 1999). We loaded BAPTA/Ca<sup>2+</sup> by waiting for their diffusion from the electrode lumen into the cell cytoplasm, which we have shown elsewhere is complete  $\sim 150$  s after attaining whole cell mode (Holcman and Korenbrot, 2004). In the experiments reported here, we began recording current data  $\sim 2.5$  min after first attaining whole cell mode.

To confirm that bass cones were effectively loaded with BAPTA, we characterized their response to light. Previous studies have demonstrated that effective cytoplasmic Ca<sup>2+</sup> buffering slows down the cone photocurrent time course and increases its photosensitivity (Nakatani and Yau, 1988; Matthews et al., 1990). The holding dark current at  $-40$  mV in BAPTA-buffered cells was  $-13.5 \pm 21.6$  pA (14 cells), not that different from the value in normal cones  $-3.2 \pm 8.9$  (17 cells). Bass cones loaded with BAPTA/Ca<sup>2+</sup> exhibited the expected changes in photocurrent kinetics and sensitivity (Fig. 2 B). In seven different cones, we found the following mean values (terms from Eq. 1.1):  $I_{max} = 27.4 \pm 16$  pA and  $\sigma = 42.3 \pm 15.3$  photons/ $\mu\text{m}^2$  (compared with  $I_{max} = 24.9 \pm 4.6$  pA and  $\sigma = 168.6 \pm 60$  photons/ $\mu\text{m}^2$  in normal cells). The mean time to peak for dim light flash photocurrents was  $185 \pm 32$  ms in BAPTA-loaded cones, but  $78 \pm 5$  ms in 11 normal ones. Thus, BAPTA is effectively loaded into the cone outer segment since photocurrents are slower and more sensitive to light. On the other hand, the mean dark holding current and peak photocurrent amplitude are not significantly changed by BAPTA/Ca<sup>2+</sup> load. These facts suggest that the dark cytoplasmic free Ca<sup>2+</sup> concentration in the patched cone outer segments is not very different from that in unperturbed cells. We will take the dark cytoplasmic level to be 400 nM, the value measured in intact cones (Sampath et al., 1999).

While in our analysis we assume that BAPTA absolutely stopped Ca<sup>2+</sup> oscillations, this is unlikely in reality. In our experimental paradigm, however, it is not necessary that Ca<sup>2+</sup> oscillations stop absolutely, just that they be attenuated sufficiently to keep GC activity from fluctuating. From the known chemical kinetics of BAPTA–Ca<sup>2+</sup> interactions, we calculate that at 10 mM BAPTA, Ca<sup>2+</sup> oscillation is attenuated by  $\sim 1/1.8 \times 10^4$ . This implies that if the mean Ca<sup>2+</sup> level is 400 nM, GC activity does not follow changes of  $\pm 0.02$  nM or smaller. Also, we only require the 10 mM BAPTA buffering system maintain Ca<sup>2+</sup> constant in the DARK, in the presence of what must be small oscillations caused by dark current noise (in balance with the Na/Ca<sup>2+</sup>,K exchanger). This is a small concentration challenge when compared with the much larger challenge caused by illumination. Thus, Ca<sup>2+</sup> buffering by BAPTA in the dark-adapted cone is effective, although its ability to clamp cytoplasmic Ca<sup>2+</sup> during intense, prolonged steps of light may be less effective.

The dark current noise in Ca<sup>2+</sup>-buffered cones is different from that in normal cones both in its amplitude and power spectrum (Fig. 2 A). In eight BAPTA-loaded cones, the mean variance of the current noise was  $0.32 \pm 0.13$  pA<sup>2</sup> in the dark and  $0.016$  pA<sup>2</sup> in the light (0–20 Hz). The power density spectrum in the presence of BAPTA is different from that in the absence of the

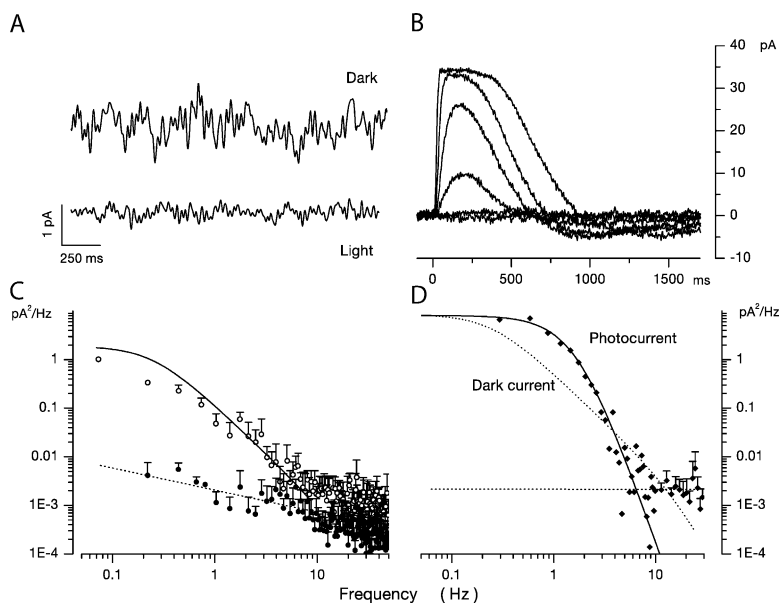


FIGURE 2. Dark noise and photocurrents in bass single cone loaded with 10 mM BAPTA at 400 nM free  $\text{Ca}^{2+}$  to attenuate fluctuation in free  $\text{Ca}^{2+}$ . Voltage-clamped membrane current measured at  $-40$  mV holding voltage. (A) Membrane current in the dark (top trace) and under continuous illumination ( $1.2 \times 10^5$  540 nm photons/ $\mu\text{m}^2$  s) (bandpass 0–40 Hz). Mean holding current in dark was  $-38.7$  pA and noise variance  $0.261$  pA<sup>2</sup>. Mean holding current in light was 1 pA and noise variance  $0.031$  pA<sup>2</sup>. (B) Photocurrent activated by 10-ms flash of 540-nm light presented at time zero. Responses generated by flashes that delivered 0.6, 2.5, 11.2, 64.5, 257, and 1,546 photons/ $\mu\text{m}^2$ . The light dependence of the photocurrent peak amplitude reached half maximum amplitude at  $\sigma = 28.4$  photons/ $\mu\text{m}^2$  (Eq. 1.1). (C) Power spectra of the fluctuations in current amplitude (noise) in darkness (open symbols) and under continuous illumination (filled symbols) shown in A. The continuous line over the data is a theoretical function based on a model of the molecular origin of the current fluctuations (Eq. 1.8). The dashed line over the data in light is a straight line

optimally fit to the data points. (D) Power spectra of the photocurrent generated by a 11.2 photon/ $\mu\text{m}^2$  photon flash shown in B. The continuous line over the data is an optimally fit product of three identical Lorentzians with  $\alpha = 1.69$  Hz. The dotted line is the function that describes dark noise spectrum (from C) shifted to match the zero frequency asymptote. It is drawn to illustrate the difference between photocurrent and dark current noise spectra.

buffer and the difference is analyzed in detail below (continuous line in Fig. 2 C, compare with Fig. 1 C). Importantly, in the presence of BAPTA, the power spectrum of dark noise is different from that of the photocurrent. The photocurrent power spectrum is well fit by the product of three Lorentzians of identical rate  $\alpha$  (continuous line in Fig. 2 D). In 12 cells, the mean value of  $\alpha$  was  $2.17 \pm 0.57$  Hz. The power spectrum of dark noise is described by a very different function (discussed below) (continuous line in Fig. 2 C), again, indicating that VP thermal excitation is not the dominant mechanism underlying dark noise.

#### *Dark Noise in Bass Single Cones Does Not Arise from Thermal Excitation of Cone Visual Pigment*

We have reasoned, in agreement with others before (Baylor et al., 1984; Rieke and Baylor, 1996), that in both normal and BAPTA/ $\text{Ca}^{2+}$ -loaded cones, thermal excitation of VP is not the dominant cause of dark current noise because the time course of the VP-initiated events is different from that of the individual events underlying current noise. But this does not mean thermal VP excitation does not occur, simply that its rate is slow compared with the dominant molecular mechanism. We attempted to uncover the relative contribution of VP thermal excitation, if any, to the observed dark noise. To this end, we measured dark current noise in cones containing significantly fewer numbers of dark VP than normal cells. If overall dark noise includes a significant contribution from spontaneous VP excitation, then reducing the number of VP in darkness

should change the power of the noise signal. Power (in watts) was measured by integrating the power spectral density between 0 and 20 Hz, a range that includes nearly in full the light-sensitive power (Figs. 1 and 2).

We reduced the number of VP molecules by briefly treating individual cell in the dark with hydroxylamine and washing extensively before starting the electrophysiological recording (see MATERIALS AND METHODS). Hydroxylamine removes 11-cis retinal from dark cone VP (dark-bleaching), but not from rod VP (Johnson et al., 1993; Kawamura and Yokoyama, 1998). Gene sequence data has identified 5 phylogenetically distinct classes of VP (Yokoyama, 1994). Only rod rhodopsin (class RH1) is impervious to hydroxylamine treatment in the dark. In every other class of VP, hydroxylamine causes loss of chromophore in darkness with a time constant of minutes to tens of minutes, depending on the molecular identity of the VP (Johnson et al., 1993; Kawamura and Yokoyama, 1998). The phylogenetic class of single bass VP is either RH2 or MWS/LWS by its wavelength of maximum absorbance (540 nm) and can be reasonably expected to dark-bleach by hydroxylamine.

Individual cones were superfused in the dark for 120 s with 60 mM hydroxylamine, followed by continuous washing for  $\sim 5$  min. After washing, dark current noise and photocurrents were measured in the treated cells with electrodes filled with BAPTA/ $\text{Ca}^{2+}$  solution. Hydroxylamine likely enters the cone cytoplasm (and leaves during washout) because it permeates through open CNG ion channels (Hackos and Korenbrot, 1999). The photocurrents recorded in treated cells were of

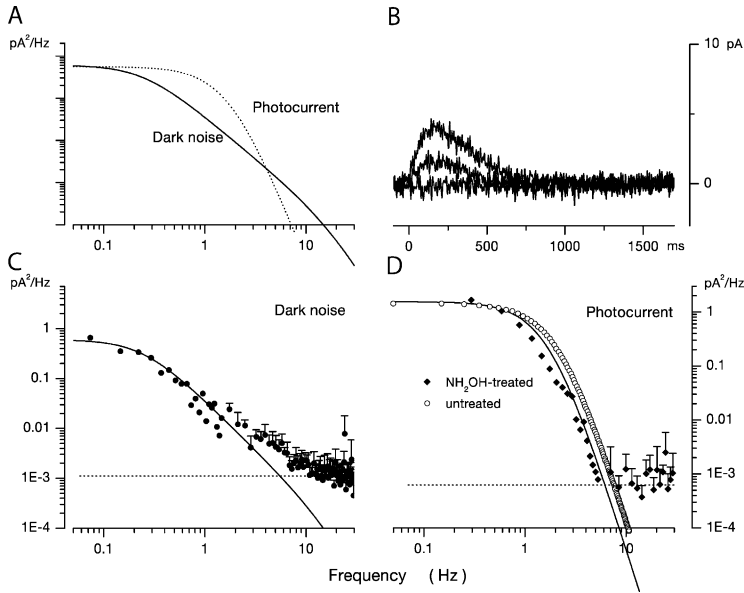


FIGURE 3. Dark noise and photocurrents in a bass single loaded with 10 mM BAPTA at 400 nM free  $\text{Ca}^{2+}$  and briefly treated with hydroxylamine to decrease the number of dark VP molecules. (A) Comparison of the power spectra of the dark noise (continuous line) and the dim light photocurrent (dotted line) in the same cell. The lines are redrawn from C and D but scaled to match their zero frequency amplitude. The panel graphically demonstrates the difference between the two power spectra. (B) Photocurrent activated by 10-ms flash of 540-nm light presented at time zero. Responses generated by flashes that delivered 233, 6,417, and 25,546 photons/ $\mu\text{m}^2$ . At the brightest light tested, the peak amplitude was only  $\sim 15\%$  of that measured in untreated cells. The loss in light sensitivity demonstrates that the treated cell lost  $>1/10^3$  VP molecules in the dark. (C) Power spectra of dark current fluctuations in the same hydroxylamine-treated cone. The continuous line over the data is an optimally fit theoretical function based on a model of the molecular origin of current fluctuations (Eq. 1.8). (D) Power spectra of the photocurrent generated by the 25,546 photon/ $\mu\text{m}^2$  photon flash shown in B. The continuous line over the data is an

optimally fit product of three identical Lorentzians with  $\alpha = 1.75$  Hz. For comparison, open circles illustrate the function that best describes the mean dim light photocurrent in untreated cones ( $\alpha = 2.17$  Hz). The near identity of the two spectra shows that transient hydroxylamine treatment does not affect the photoresponse of bass cones, although they are much less sensitive to light.

normal time course and their peak amplitude increased with light intensity (Fig. 3 B). We did not find light-unresponsive cells. The cones, however, were substantially less sensitive to light than normal ones. At the brightest flash intensity possible in our instrument ( $2.5 \times 10^4$  540 nm photons/ $\mu\text{m}^2$ ), photocurrents were comparable in peak amplitudes to those generated by 10–20 photons/ $\mu\text{m}^2$  flashes in normal cones. That is, dark hydroxylamine treatment resulted in photocurrents of typical time course, but  $\sim 1/10^3$  as light sensitive as those in untreated cones.

We emphasize that dark hydroxylamine treatment was brief and the reagent was extensively washed out of the cells before dark noise or photocurrents were measured. This is important since photoresponses are altered by the presence of hydroxylamine because it accelerates the decay rate of metarhodopsin II (Pepperberg and Okajima, 1992; Leibrock and Lamb, 1997). Hydroxylamine-treated cones had a dark current amplitude within the range of that of untreated cells (mean dark current was  $-1 \pm 8.8$  pA,  $n = 5$ ), indicating that dark cGMP and  $\text{Ca}^{2+}$  concentrations were unchanged. Also, the photocurrent kinetics of hydroxylamine-treated cells was indistinguishable from that of normal cells. This is qualitatively demonstrated by comparing the time course of data in Fig. 2 B and Fig. 3 B. Quantitatively, the data in Fig. 3 D show that photocurrent power spectra recorded in hydroxylamine dark-treated cones were the same as those measured in untreated cones. Photocurrent power spectra in hydroxylamine-treated cells were well fit by the product of three identical Lorentzians with average characteristic frequency  $1.63 \text{ Hz} \pm 0.67$

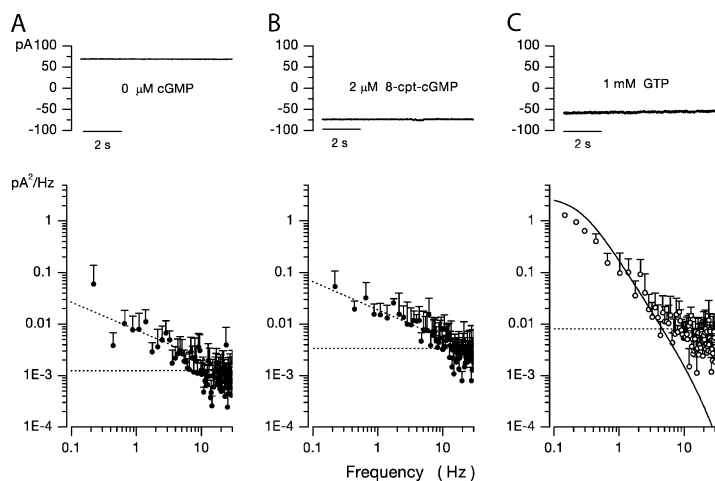
( $n = 3$ ). These are the same function and similar characteristic frequencies to those that describe normal photocurrents. In normal cells, the average characteristic frequency was  $2.17 \pm 0.57$  Hz ( $n = 12$ ). Finally, hydroxylamine treatment did not alter the cone's voltage-gated currents (unpublished data). Thus, there is no evidence of unanticipated pharmacological effects. Brief dark hydroxylamine treatment reduces the number of VP pigment (and thus sensitivity) without evidently affecting the biochemical phototransduction cascade.

Since photoreceptor sensitivity is proportional to VP concentration, loss of photosensitivity indicates our hydroxylamine treatment caused chemical bleaching of  $\sim 999$  out of every  $10^3$  VP molecules. The absorption cross section,  $x_s$ , of a single bass cones illuminated on its side with unpolarized, 540 nm light is given by (Baylor et al., 1979; Miller and Korenbrot, 1993)

$$x_s = 2.3 \text{COS}_{vol} Q_{eff} OD_T \left(1 + \frac{1}{r}\right),$$

where outer segment volume  $\text{COS}_{vol}$  is  $125 \mu\text{m}^3$ . In fish, transverse specific optical density  $OD_T$  is  $0.016 \text{ OD}/\mu\text{m}$  and dichroic ratio  $r$  is 4.06 (Harosi, 1976). For unpolarized light  $f = 0.5$  and quantum efficiency of bleaching  $Q_{eff}$  is 0.67. In a normal single cone  $x_s = 1.92 \mu\text{m}^2$ . Our hydroxylamine treatment reduced  $x_s$  to  $0.00195 \mu\text{m}^2$ ; since the cell geometry is unchanged this means that only 1 out of every 1,000 dark VP originally present remains available to capture photons.

Jones et al. (1996) suggested that light-bleached VP can cause light adaptation as made evident by a speeding up of the photocurrent kinetics in rods in which a



1 mM GTP and 3 mM ATP. Holding current in dark was  $-54$  pA. The bottom panel illustrates the power spectrum of the dark noise. It is well described by Eq. 1.8, the continuous line optimally fit to experimental data. Dark noise in BAPTA-loaded cones is detected only in the presence of cGMP and originates from fluctuations in PDE activity.

significant fraction of VP had first been bleached by light ( $>0.1\%$ ). Since cone photocurrents we measured following hydroxylamine treatment have essentially the same kinetics as those of normal, dark-adapted photoreceptors, we infer that hydroxylamine-bleached VP molecules do not, themselves, cause light adaptation.

Hydroxylamine treatment did not detectably affect the power spectral density of the dark noise, illustrated in Fig. 3 C. The spectra were well fit by the same mathematical function (continuous line in Fig. 3 B) that describes the noise in untreated cells (detailed below). More important, the time-averaged power of the dark noise in treated and untreated cells was not different. Mean average power in treated cells was  $0.32 \pm 0.14$  pA<sup>2</sup> ( $n = 6$ ) and it was  $0.32 \pm 0.09$  pA<sup>2</sup> ( $n = 5$ ) in treated cells. These values are not statistically different (two-tailed Student's *t* test). Thus, reducing the number of dark VP molecules does not change the frequency or power characteristics of the dark noise power spectral density. These are the anticipated results that affirm that spontaneous excitation of VP molecules is not the dominant cause of dark current fluctuations in bass single cones.

#### *Dark Current Noise in Ca<sup>2+</sup>-buffered Cones Originates from Fluctuation in Phosphodiesterase Activity*

To demonstrate that dark current variance indeed arises from cGMP fluctuations in Ca<sup>2+</sup>-buffered cones, we measured current noise in BAPTA-loaded cells in the absence of added GTP and ATP. In the absence of triphosphate nucleotides, there is no cGMP synthesis, and after endogenous cGMP is consumed, CNG ion channels in the outer segment close. This is manifested by a slow change in holding current at  $-40$  mV from its starting value near 0 to a steady positive value, a mea-

sure of outward current flow through Kv channels in the inner segment. In striped bass single cones, this stationary condition is reached  $\sim 150$  s after attaining whole cell mode (Rebrük et al., 2000; Holcman and Kornbrot, 2004).

The mean dark holding current at  $-40$  mV in cones loaded with BAPTA/Ca<sup>2+</sup> without GTP and ATP and measured 2.5 min after establishing whole cell mode or thereafter was  $42.8 \pm 21.6$  pA (five cells). The mean variance of the current noise was  $0.037 \pm 0.012$  pA<sup>2</sup> (0–20 Hz) and, of course, it was light insensitive. This noise variance is essentially the same as that measured under continuous light in BAPTA-loaded cones when endogenous cGMP level is also zero ( $0.016 \pm 0.005$  pA<sup>2</sup>). Moreover, the dark noise power spectra in the absence of cGMP (Fig. 4 A) (five cells) or in the presence of continuous light (Fig. 2 C) (seven cells) are essentially the same. These results demonstrate that light-sensitive dark current noise is strictly dependent on the presence of cGMP.

We tested the hypothesis that fluctuations in PDE activity alone are the dominant source of dark noise in BAPTA-loaded cones. To this end, we measured current fluctuations in BAPTA-loaded cones in the presence of the cGMP analogue 8-cpt-cGMP (8-p-chlorophenylthio-cGMP) and the absence of added GTP or ATP. 8-cpt-cGMP is an effective CNG channel activator, but not a PDE substrate over the same concentration range (Wei et al., 1998). At  $-40$  mV and in the absence of divalent cations, 8-cpt-cGMP half-maximally activates CNG channels in bass cone detached membrane patches at  $\sim 5$   $\mu$ M (unpublished data).

Cones loaded with BAPTA/Ca<sup>2+</sup> and 2  $\mu$ M 8-cpt-cGMP (without GTP or ATP) exhibited an inward current that slowly and continuously increased over time

(mean rate  $-1.27$  pA/s, five cells). A steady state was not reached and, eventually, the current was so large (hundreds of pA) that cells were irreversibly damaged. The inability to reach equilibrium likely reflects the fact that 8-cpt-cGMP is membrane permeable, and, in effect, there is a never ending flow from pipette lumen to cell cytoplasm to the bathing solution across the cell membrane. Experimentally we defined a quasi steady state by continuously monitoring current amplitude and measuring noise when current magnitude was near  $-100$  pA (Fig. 4 B). For five cells analyzed, the mean holding current at  $-40$  mV was  $-82 \pm 16.5$  pA and the drift rate  $-1.27 \pm 0.9$  pA/s. Calculations indicate that under these conditions, the number of active CNG channels was about three times the number normally active in darkness (when outer segment inward current is about  $-30$  pA).

The power spectrum of dark current activated by 8-cpt-cGMP in BAPTA/Ca<sup>2+</sup>-loaded cones (Fig. 4 B) appears essentially the same as that measured in the absence of cGMP, achieved either by omitting GTP and ATP (Fig. 4 A) or in a normal cell under continuous, saturating light (Fig. 2 C). Current noise activated by 8-cpt-cGMP exhibits weak  $1/f$  dependence  $<30$  Hz and is frequency independent  $>30$  Hz. It is not fit by the function that describes the noise in normal, BAPTA/Ca<sup>2+</sup>-loaded cones (Fig. 4 C). The same results were obtained in five different cells. That is, the nonhydrolyzable cGMP analogue activates CNG channels, but its concentration does not fluctuate because it is not hydrolyzed and, hence, cannot reflect PDE dynamics. When cGMP is present, channels are also open, but current noise is much larger, reflecting cGMP hydrolysis and PDE dynamics. These observations demonstrate that cGMP fluctuations caused by PDE activity are the principal source of current dark noise  $<30$  Hz in Ca<sup>2+</sup>-buffered single cones.

#### A Theory to Model Dark Current Noise

We present a model that assumes thermal fluctuations in the number of active PDE molecules in darkness and computes the consequent fluctuations in cytoplasmic cGMP concentration and the outer segment membrane current. Details of mathematical derivations and an analysis of the equations are presented in APPENDIX. Here we outline the features of the conceptual model and its mathematical expression.

We assume that the total number of PDE molecules in the cone outer segment,  $N_0$ , is constant and distributes between active,  $N^*$ , and inactive states,  $N$ , due to thermal activation. Activation events are independent from each other, and the transition between inactive and active states occurs with forward activation rate  $k_a$  and reverse inactivation rate  $\tau^{-1}$ :



where  $N_0 = N + N^*$ .

We show in Appendix 1 that the dynamics of the number of active PDE is well described by the following effective stochastic equation:

$$dN^* = (\alpha_1 - \alpha_2 N^*)dt + \sigma_0 dw, \quad (1.4)$$

where  $\alpha_1 = k_a N_0$  and  $\alpha_2 = (1/\tau + k_a)$ ,  $\sigma_0$  is variance, and  $dw$  is the standard centered Brownian motion of variance 1.

Cytoplasmic free cGMP concentration is controlled by the balanced activity of PDE and GC. The reaction rates of each of these enzymes have been thoroughly investigated (for reviews see Pugh and Lamb, 2000; Ebrey and Koutalos, 2001). The total concentration of cGMP, denoted as  $C(t)$ , fluctuates according to

$$\frac{dC(t)}{dt} = -\frac{k_{CAT}}{K_{mcGMP}} N^*(t) C(t) + \frac{\gamma_{max}}{1 + (Ca(t)/K_{aCa})^2}, \quad (1.5)$$

where the first term in Eq. 1.5 is the PDE hydrolysis rate and the second term is the GC synthesis rate. Following standard enzyme kinetics nomenclature,  $k_{CAT}$  is the hydrolysis turnover rate per active PDE molecule,  $K_{mcGMP}$  is the cGMP Michaelis-Menten constant of PDE, and  $N^*(t)$  is the number of active PDE molecules.  $\gamma_{max}$  is the GC maximum reaction rate,  $Ca(t)$  is the cytoplasmic free Ca<sup>2+</sup> concentration, and  $K_{aCa}$  is the Ca<sup>2+</sup> concentration at half maximal GC activation. At a fixed Ca<sup>2+</sup> concentration, Eq. 1.5 becomes

$$\frac{dC(t)}{dt} = -k_{sub} N^*(t) C(t) + \gamma, \quad (1.6)$$

where

$$k_{sub} = \frac{k_{CAT}/2}{K_{mcGMP}}$$

$k_{CAT}$  is divided by two because the active PDE holoenzyme is a dimer (for review see Beavo, 1995).

In Appendix 2, we show that the power spectrum of steady-state fluctuations in cGMP concentration can be computed from Eqs. 1.4 and 1.6 and is given by

$$S(\omega) = S_1(\omega) S_2(\omega) = \frac{(k_{sub} C_0)^2 \sigma_0^2}{16} \frac{1}{\omega_1^2 + \omega^2} \frac{1}{\omega_2^2 + \omega^2}. \quad (1.7)$$

This is the product of two Lorentzians each of characteristic frequencies  $\omega_1 = \alpha_2 = k_a + \tau^{-1}$ , and  $\omega_2 = k_{sub} N_d^*$ , where  $N_d^*$  is the mean number of active PDE molecules in the dark.

From the known dependence of current on cGMP concentrations in bass cones (APPENDIX, Eq. A2.7) (Korenbrodt and Rebrink, 2002), the power spectrum of the dark current,  $S_1(\omega)$ , is given by

$$S_1(\omega) = 9 C_0^4 (I_{max}/K_{1/2cG})^2 S(\omega), \quad (1.8)$$

where  $I_{max}$  is the maximum possible current amplitude,  $K_{1/2cG}$  is the cGMP concentration that half maximally activates current at a fixed  $Ca^{2+}$  concentration, and  $n$  is a parameter to reflect cooperative channel activation by cGMP.

#### Mean Dark Activities of PDE and GC in Bass Cones

Eqs. 1.7 and 1.8 state that if thermal fluctuations of PDE are the cause of dark noise, then in BAPTA/ $Ca^{2+}$ -loaded cones, the power spectrum of dark current fluctuations should be described by the product of two Lorentzians of characteristic frequencies  $\omega_1$  and  $\omega_2$ . The dark noise power spectrum is, indeed, fit by the product of two Lorentzians, but the values  $\omega_1$  and  $\omega_2$  cannot be simply determined by matching experimental and theoretical data because more than one combination of values for these parameters achieves successful match.

To make a more certain determination of PDE chemical kinetics, we first measured directly the value of  $\omega_2$  in bass cones. Recall from Eqs. 1.6 and 1.7 that  $\omega_2 = k_{sub}N_d^* = \beta_{dark}$ .  $\beta_{dark}$  is the steady-state cGMP hydrolysis rate in the dark. In darkness, rates of cGMP synthesis and hydrolysis are equal and opposite each other. If cGMP synthesis or hydrolysis are instantly blocked, the nucleotide concentration (and hence the dark membrane current) will change with a time course determined by the activity of the unblocked enzyme.  $\beta_{dark}$  was first measured in rods by Hodgkin and Nunn (1988) who demonstrated that blocking GC (by suddenly elevating cytoplasmic  $Ca^{2+}$ ) or PDE (with the enzyme inhibitor IBMX) yields essentially the same result.

In dark-adapted BAPTA/ $Ca^{2+}$ -loaded bass cones, we measured the dark rate of cGMP synthesis. We recorded the change in membrane current caused by the sudden suppression of PDE activity with 200  $\mu$ M zaprinast, a membrane-permeable PDE blocker ( $IC_{50} = 125$  nM) (Gillespie and Beavo, 1989). In any given trial, we first established that the cell under study functioned normally by evaluating its dark current noise and flash photocurrents. We then measured the effect of rapidly ( $\leq 50$  ms) changing the solution bathing the cell to Ringer's containing zaprinast. Fig. 5 illustrates typical results observed in every cell studied ( $n = 4$ ). The cells' photocurrents (Fig. 5 A) and dark current noise (Fig. 5 B) were indistinguishable from those of a larger population of normal cones. For this small set, peak photocurrent amplitude was  $28 \pm 1.1$  pA, time to peak  $93 \pm 6.9$  ms, and photosensitivity  $184.2 \pm 37$  photons/ $\mu$ m<sup>2</sup>. Upon switching to the zaprinast-containing solution, the inward current increased linearly up to a limiting, steady value (Fig. 5 C). The linear rate of current increase reflects the controlling activity of GC; as cGMP raises, so does the current. As time progresses and the current increases, cytoplasmic free  $Ca^{2+}$  also raises

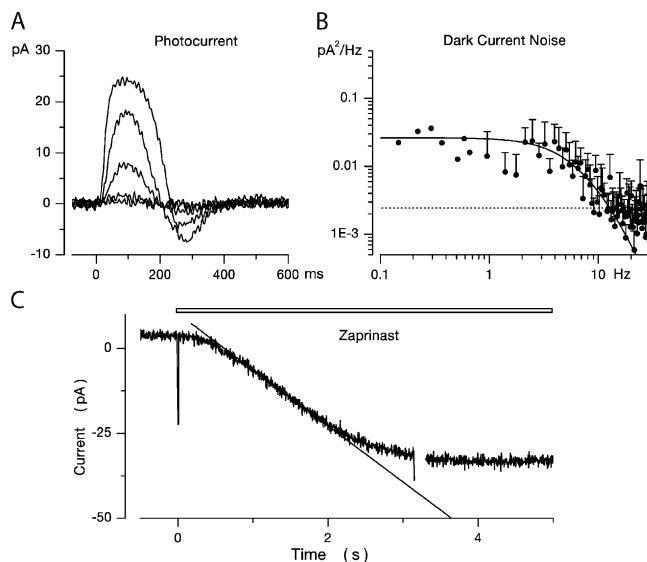


FIGURE 5. The effect of zaprinast superfusion on the holding current of a normal bass single cone in the dark. Voltage-clamped membrane currents measured in the same cell at  $-40$  mV holding voltage. The mean holding current in dark was 8.2 and the noise variance 0.274 pA<sup>2</sup>. (A) Photocurrent activated by 10-ms flash of 540-nm light presented at time zero. Responses generated by flashes that delivered 2.4, 10.8, 62, 242, and 1,486 photons/ $\mu$ m<sup>2</sup>. The light dependence of the photocurrent peak amplitude reached half maximum amplitude at  $\sigma = 146$  photons/ $\mu$ m<sup>2</sup> (Eq. 1.1). (B) Power spectra of the dark noise. The continuous line over the data in darkness is a function derived from a theoretical model of the molecular origin of the current fluctuations (Eq. 1.13). (C) At time = 0, the solution bathing the cone was rapidly ( $< 50$  ms) switched to one containing 200  $\mu$ M zaprinast, a membrane-permeable blocker of PDE activity. The inward holding current increased linearly at first and then reached a new stationary value. The slope of the linear current change near  $t = 0$  was  $-16.6$  pA/s. From this slope, we computed the rate of cGMP synthesis in the dark,  $\gamma_{dark} = 4.89$   $\mu$ M/s (Appendix 3).

which, in turn, reduces  $Ca^{2+}$ -dependent GC activity. A new stationary conditioning is reached with a balance between the new, reduced rate of synthesis and the diffusional loss of cGMP from the outer segment into the patch pipette.

The time course of the zaprinast-dependent current change is obtained from the solution of a system of equations (detailed in Appendix 3) that describe the chemical reaction when PDE reaction rate is zero. We show that the value of the dark GC activity,  $\gamma_{dark}$ , can be explicitly computed from the tangent at  $t = 0$ . Only near zero is the computation possible since it is based on the presumption that only the initial (linear) rate of current increase is defined by GC activity alone. As time progresses and cytoplasmic  $Ca^{2+}$  rises, the initial conditions change. In the experimental data (Fig. 5 C), there is a brief delay between the addition of zaprinast and the linear change in membrane current, most likely time required for zaprinast to permeate and accumu-

late within the cell. The slope of the tangent fit to the initial rate of current rise was  $21.1 \pm 6$  pA/s ( $N = 4$ , range 16.6–29.6 pA/s) (Fig. 5), from which we calculate a mean cGMP synthesis rate in darkness,  $\gamma_{dark} \pm 1.7$   $\mu$ M cGMP/s.

By definition,  $\gamma_{dark} = \beta_{dark} C_0$ , where  $C_0$  is the cytoplasmic cGMP concentration in darkness.  $C_0$  is  $\sim 25$   $\mu$ M, calculated from the relationship between dark current amplitude and cGMP concentration (Eq. 1.10;  $K_{cG}$  at 400 nM  $Ca^{2+}$  is  $\sim 135$   $\mu$ M cGMP and  $n = 2.5$ ), given that mean dark outer segment current is  $\sim 30$  pA and this is  $\sim 2\%$  of  $I_{max}$  (Cobbs et al., 1985; Rebrik et al., 2000). From the measured  $\gamma_{dark}$  value we compute mean  $\beta_{dark} = 0.25 \pm 0.06$  s $^{-1}$ .

The experimental data in Fig. 5 C can also be analyzed to yield the value of  $\beta_{dark}$  with a simpler algorithm proposed by Hodgkin and Nunn (1988). This algorithm requires independent knowledge of the cooperative dependence of cGMP-dependent current on cGMP concentration (Eq. 1.10), a value = 2.5 in bass cones. Analysis of our data with the Hodgkin and Nunn algorithm yields  $\beta_{dark} = 0.27 \pm 0.06$  s $^{-1}$ .

#### Rates of PDE Activation and Inactivation in Bass Cones

From the experimental  $\beta_{dark}$  value, we assigned  $\omega_2 \equiv 0.248$  Hz. We then fit Eq. 1.8 to the dark current power spectra measured in  $Ca^{2+}$ -buffered cones with the value of  $\omega_1$  as the sole adjustable parameter (and a scaling coefficient to match the zero frequency power). Panels in Figs. 2, 4, and 6 illustrate the computer-aided, nonlinear least-squares fit of theoretical and experimental data in five different cells and demonstrate the range of the adequacy of the fit. The chi-square minimization in the fitting algorithm yields an estimate of the error in the value of the  $\omega_1$  parameter. In all cells analyzed this error was  $\leq 10\%$ . To illustrate conservatively the range of the error in the optimum value of the adjustable parameter  $\omega_1$ , we plot in Fig. 6 (top panel) the optimal function, as well as two other functions in which the value of  $\omega_1$  is 20% larger and smaller than the optimum. These lines demonstrate the confidence limits of the fit. The error in the fit of any one power spectra is less than the error from differences among the cells in our sample. For 11 cones, the mean value of  $\omega_1$  was  $18.53 \pm 4.41$  Hz.

Knowing the values of  $\omega_1$  and  $\omega_2$ , the following computations are possible. From the definition  $\omega_2 = k_{sub} N_d^* = 0.25$  s $^{-1}$  and the biochemically determined value of  $k_{sub}$  (Table I), we calculate the mean number of active PDE in darkness,  $N_d^* \sim 60$  (Table II). In the steady-state, solution of Eq. 1.4 (from Appendix 1) yields

$$N_d^* = N_0 \frac{k_a}{\tau^{-1} + k_a}, \quad (1.9)$$

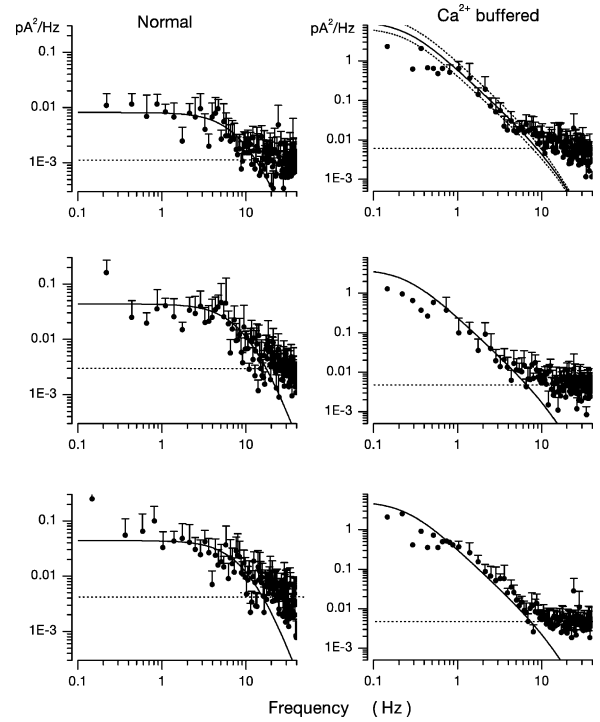


FIGURE 6. Dark noise power spectra measured in different bass cones. Experimental data are in symbols and the continuous line is optimally fit theoretical function based on a model of the molecular origin of the dark noise. On the left are data measured in normal cells. On the right are data measured in cones loaded with 10 mM BAPTA at 400 nM free  $Ca^{2+}$ . The top panel on the right illustrates both the optimally fit theoretical function and confidence limits if the value of the single adjustable parameter,  $\omega_1$ , were 20% larger or smaller than optimized by the fitting algorithm.

where  $N_0$  is the total number of PDE molecules in a bass cone outer segment.  $N_0 = 3 \times 10^6$  molecules, since PDE concentration in a cone is  $\sim 1/70$  that of the VP (Zhang et al., 2003), VP concentration in fish cones is 3.3 mM (Harosi, 1976) and the volume of a single bass cone outer segment is 0.1 pL (Holcman and Korenbrot, 2004). From the definition  $\omega_1 = k_a + \tau^{-1} = 18.53$  s $^{-1}$  and Eq. 1.9, we compute the rates of cone PDE activation and inactivation to be  $k_a = 3.7 \times 10^{-4}$  s $^{-1}$  and  $\tau^{-1} = 18.5$  s $^{-1}$  (Table II).

The meaning of these kinetic rates is highlighted by comparing our data with results of investigations of dark PDE kinetics previously measured in rods of non-mammalian species (Table II). The mean rate of dark PDE activity,  $\beta_{dark} = k_{sub} N_d^*$ , in intact tiger salamander rods was found to be 2 s $^{-1}$  by Hodgkin and Nunn (1988) and anywhere between 0.9 and 1.6 s $^{-1}$  (mean 1.2) by Nikonov et al. (2000). In toad rods, this rate is  $\sim 1.8$  s $^{-1}$  (Rieke and Baylor, 1996). The total number of active PDE molecules in darkness is higher in toad or salamander rod outer segment than bass cone outer segment, this difference, however, reflects their size difference. In both receptor types, the ratio of dark active

T A B L E I

*Biochemical and Biophysical Constant Used in the Analysis of Dark Current Noise in Bass Single Cones*

Subject	Parameter	Symbol	Units	Value
PDE	Molecular turnover <sup>a</sup>	$k_{CAT}$	$\mu\text{Ms}^{-1}$ in cone OS	$8.2 \times 10^{-2}$
			Molecules per second	$5 \times 10^3$
	Michaelis-Menten constant for cGMP <sup>b</sup>	$K_{mcGMP}$	$\mu\text{M}$	10
			Molecules in cone OS	$6 \times 10^5$
GC	Gain between excited VP and active PDE <sup>b</sup>	$V_{PDE}$	PDE* per second per VP*	125
	Maximum activity <sup>c</sup>	$\gamma_{max}$	$\mu\text{Ms}^{-1}$	100
	Ca <sup>2+</sup> concentration at half maximal activation <sup>c</sup>	$K_{aCa}$	$\mu\text{M}$	0.1
	Cooperativity index	$n$		2
cGMP-dependent current	Maximum dark current	$I_{max}$	pA	2,500
	Minimum cGMP concentration at half maximal activation <sup>d</sup>	$K_{cGmin}$	$\mu\text{M}$	50
	Maximum cGMP concentration at half maximal activation <sup>d</sup>	$K_{cGmax}$	$\mu\text{M}$	316
	Ca <sup>2+</sup> binding constant <sup>d</sup>	$K_{Ca}^f$	$\mu\text{M}$	0.86
	cGMP cooperativity index <sup>d</sup>	$n$		2.5
Ca <sup>2+</sup> dynamics	Ca <sup>2+</sup> fraction of CNG current <sup>e</sup>	Pf	$I_{Ca}/I_{total}$	0.35
	Instantaneous Ca <sup>2+</sup> buffer power <sup>f</sup>	$\Omega$	Ca <sup>2+</sup> free/total Ca <sup>2+</sup>	0.15

<sup>a</sup>Dumke et al., 1994; D'Amours and Cote, 1999; Leskov et al., 2000.

<sup>b</sup>Leskov et al., 2000.

<sup>c</sup>We arrive at this value in cones from our measurement of  $\gamma_{dark} = 6.22 \mu\text{M/s}$  at 400 nM Ca<sup>2+</sup> using Eq. 1.5. This result is consistent with measured values in rod GC, which range between 60 and 100  $\mu\text{M/s}$  (for reviews see Pugh and Lamb, 2000; Ebrey and Koutalos, 2001).

<sup>d</sup>Rebrik et al., 2000.

<sup>e</sup>Ohyama et al., 2000.

<sup>f</sup>Miller and Korenbrot, 1993.

PDE over total PDE,  $N_d^*/N_0$ , is not that different. In both cell types, PDE activation is very fast and of essentially identical rate. The inactivation rate, however, is 5–10 times faster in cones than rods. Because the inactivation rate is so much slower than activation, it determines the lifetime of the active PDE state ( $\tau = 1/[k_a + \tau^{-1}]$ ). These results mean that at room temperature in nonmammalian, intact photoreceptors, the lifetime of dark active PDE is between 0.5 and 1.1 s in rods, but it is only  $\sim 50$  ms in cones.

*Dark Current Noise in Normal Cones*

To understand dark noise in a normal cone, we extended the theoretical model to include Ca<sup>2+</sup> dynamics. Cytoplasmic Ca<sup>2+</sup> in the outer segment is regulated by the kinetic balance between Ca<sup>2+</sup> influx through the CNG ion channels and its efflux through Na/Ca,K exchangers (Yau and Nakatani, 1985; Miller and Korenbrot, 1987). Free Ca<sup>2+</sup> regulates GC activity (Koch and Stryer, 1988; Gorczyca et al., 1995), and in cones, but not rods, it also regulates the ligand sensitivity of the CNG channels (Rebrik and Korenbrot, 1998; Rebrik et al., 2000).

When Ca<sup>2+</sup> concentration fluctuates, the dynamics of cGMP concentration is given by Eq. 1.5. The cGMP dependence of outer segment current is Ca<sup>2+</sup> dependent and given by (Rebrik et al., 2000)

$$I_m(t) = I_{max} \frac{C(t)^n}{C(t)^n + K_{1/2cG}^n(Ca(t))}, \quad (1.10)$$

where  $K_{1/2cG}(Ca)$  is the Ca<sup>2+</sup>-dependent value of the cGMP concentration at half maximal current and  $n$  denotes the cooperative interaction of cGMP in channel activation. Empirical fit to experimental data shows that the dependence of cGMP sensitivity on Ca<sup>2+</sup> is well described by the function (Rebrik et al., 2000)

$$K_{1/2cG}(Ca(t)) = K_{1/2cGmin} + \frac{(K_{1/2cGmax} - K_{1/2cGmin})Ca(t)}{Ca(t) + K_{Ca}}, \quad (1.11)$$

where  $K_{1/2cGmin}$  and  $K_{1/2cGmax}$  are minimum and maximum values, and  $K_{Ca}$  is a Ca<sup>2+</sup> binding constant (Table I). The dynamics of cytoplasmic free Ca<sup>2+</sup>, denoted by  $Ca(t)$ , are described by the balance between its influx

T A B L E II

<i>Kinetics of PDE Activation and Inactivation in Retinal Photoreceptors</i>							
	$\beta_{dark}$	$N_d^*$	$N_0$	$N_d^*/N_0$	$k_a$	$\tau^{-1}$	$\tau$
	$s^{-1}$				$s^{-1}$	$s^{-1}$	ms
Bass cone	0.24	60	$3 \times 10^6$	$1/5 \times 10^4$	$3.7 \times 10^{-4}$	18.5	54
Rod	1–2 <sup>a,b</sup>	487	$2 \times 10^7$	$1/4 \times 10^4$	$2.7 \times 10^{4b}$	1.8 <sup>b</sup>	555

$N_d^*$ , number of active PDE molecules in dark;  $N_0$ , total number of PDE molecules in the outer segment (1/70 PDE/VP, Zhang et al., 2003);  $k_a$ , PDE forward activation rate;  $\tau^{-1}$ , PDE backward activation rate;  $\tau = 1/(k_a + \tau^{-1})$ , active PDE lifetime.

<sup>a</sup>Hodgkin and Nunn, 1988, and Nikonov et al., 2000, in tiger salamander retina.

<sup>b</sup>Rieke and Baylor, 1996, in toad retina.

and efflux and an intracellular buffer of power  $\Omega$ , the ratio of free/total  $\text{Ca}^{2+}$  (Miller and Korenbrot, 1987; Sneyd and Tranchina, 1989; Miller and Korenbrot, 1993). If the kinetics of buffering are assumed to be fast compared with the rate of  $\text{Ca}^{2+}$  entry, then  $Ca(t)$  is given by

$$\frac{dCa(t)}{dt} = J_{in}(t) - J_{eff}(t) \quad (1.12)$$

$$J_{in}(t) = P_f \frac{\Omega}{zF} J_m(t)$$

and

$$J_{eff}(t) = \phi Ca(t),$$

where  $J_{in}$  and  $J_{eff}$  are the  $\text{Ca}^{2+}$ -specific inward and outward membrane fluxes.  $P_f$  is the fraction of the current carried by  $\text{Ca}^{2+}$  (Ohyama et al., 2000),  $\Omega$  is cytoplasmic  $\text{Ca}^{2+}$ -buffering power,  $zF$  are valence and Faraday's constant, and  $\phi$  is the time constant of outer segment  $\text{Ca}^{2+}$  clearance via the Na/Ca,K exchanger (time to reduce free  $\text{Ca}^{2+}$  to  $1/e$  of its initial value). The values of these parameters are known from biochemical and biophysical literature and are collected in Table I. The system of Eqs. 1.10–1.13 (referred to as  $S_c$ ) describes the coupled dynamics of PDE, cGMP, and  $\text{Ca}^{2+}$  cytoplasmic concentration in darkness. The system  $S_c$  is analyzed in Appendix 4. We show that the power spectrum of the dark noise, computed by linearizing the system around the steady state, is given by

$$S_f(\omega) = \frac{\sigma_0^2/4}{\omega^2 + \omega_1^2} \frac{(k_{sub}c_0)^2/4}{\left(\omega_2 + \frac{\theta\phi}{\phi^2 + \omega^2}\right)^2 + \omega^2 \left(1 - \frac{\theta}{\phi^2 + \omega^2}\right)^2}, \quad (1.13)$$

where

$$\theta = \frac{2D_1 Ca_0}{(K_{Ca}^{GC})^2} \left[ \frac{\gamma_{max}}{1 + \frac{(Ca_0)^2}{(K_{Ca}^{GC})^2}} \right]$$

and

$$D_1 = I_{max} \Omega P_f \frac{n c_0^{n-1}}{(K_{cGMP}(Ca))^n}.$$

Expression 1.13 defines the power spectrum of dark current noise in normal cones. Although it includes several independent parameters, the values of all but one of these parameters is known from data available in the biochemical and biophysical literature. We assigned the values listed in Table I. We set  $\omega_1$  and  $\omega_2$  to the values measured in  $\text{Ca}^{2+}$ -buffered cells, which simply assumes that PDE fluctuations are the same in the presence or absence of  $\text{Ca}^{2+}$  oscillations. The only freely adjustable parameter to match experimental data with the theoretical function (Eq. 1.13) is  $\phi$ , the exponential rate of  $\text{Ca}^{2+}$  clearance from the outer segment. Pan-

els in Figs. 1, 5, and 6 illustrate the fit of theoretical and experimental data in five different cells and demonstrate the range of the adequacy of the match. As discussed above, the accuracy of the single adjustable parameter used to obtain the fits as shown is conservatively  $<20\%$ , which is less than the error due to variation among sampled cells. For a total of 10 cones, the mean value of  $\phi$  was  $52.5 \pm 12.3 \text{ s}^{-1}$ . Remarkably, this value, arrived at by optimal fitting of bass cone data, is close to the rate constant measured directly in other cones, where it ranges between 10 and  $65 \text{ s}^{-1}$  (Hestrin and Korenbrot, 1990; Perry and McNaughton, 1991; Sampath et al., 1999).

## DISCUSSION

A combination of experimental data and theoretical modeling allows us to conclude that in the 0–30 Hz range, outer segment dark current noise in bass cones originates from simultaneous fluctuations in cytoplasmic cGMP and  $\text{Ca}^{2+}$  and not from thermal excitation of cone opsin. Fluctuations in cGMP arise from the dynamics of PDE thermal activation and  $\text{Ca}^{2+}$ -dependent GC activation. Under voltage clamp, variance of dark current fluctuations is  $\sim 0.23 \text{ pA}^2$ , and this is larger than the extrapolated single photon photocurrent amplitude in the same cells, 0.08 pA. This small signal to noise ratio explains why bass single cones require coincident absorption of three to seven photons to generate a detectable photocurrent.

Our results do not exclude the possibility that thermal cone opsin excitation also occurs in bass single cones, simply that the rate of this excitation is small compared with the rate of fluctuation in PDE and GC activity. Our finding in bass single cones applies to most cones investigated to date. In several different species, the dark noise power spectrum is different than that of the photocurrent (Lamb and Simon, 1977; Schnapf et al., 1990; Schneeweis and Schnapf, 1999; Rieke and Baylor, 2000). There are exceptions, however, in tiger salamander L cones (Rieke and Baylor, 2000; Sampath and Baylor, 2002) or in *Xenopus* transgenic rods expressing cone opsin (Kefalov et al., 2003) spontaneous cone opsin excitation is the molecular process that limits dark noise. It is not surprising that in different cones, dark current noise (and hence signal threshold) may be set by different limiting molecular events. Unlike rods, which are single photon detectors in every species studied to date, the absolute signal threshold is not the same in cones of different species, not even in different cones of the same species. In striped bass retina, for example, twin cones are  $\sim 10$ -fold less sensitive than single cones, and there are at least two subclasses of twin cones distinguishable by their kinetics and sensitivity (Miller and Korenbrot, 1993).

We developed a theoretical model to quantitatively analyze the feature of the dark noise. The set of equations we derived for cones averaged over space are comparable to those derived by Rieke and Baylor (1996) in their study of the continuous component of dark noise in toad rods. The two notable differences in the equation set are (1) the need to include  $\text{Ca}^{2+}$  feedback control on CNG channel ligand sensitivity in cones, but not rods, and (2) because of their geometrical differences, the effective diffusion of cGMP is not linear in cone outer segment, but linear in rods (Holzman and Korenbrot, 2004).

In  $\text{Ca}^{2+}$ -buffered cones, the power spectrum of dark noise is the product of two Lorentzians with characteristic frequencies determined by PDE activation kinetics. By fitting experimental data with analytic expressions, we determined the time constant of PDE activation and deactivation (Table II). Comparing our results with those of Rieke and Baylor (1996) in rods (Table II) supports an important insight: PDE transitions from active to inactive states are  $\sim 10$ -fold faster in cones than in rods, and the mean lifetime of an active PDE molecule is  $\sim 54$  ms in cones, but 555 ms in rods.

We extended the model to predict power spectra of dark current in normal cones. The extended model includes fluctuations in GC activity caused by changing cytoplasmic  $\text{Ca}^{2+}$ . The adequacy of the theoretical model is strengthened by the finding that the 20 ms time constant of  $\text{Ca}^{2+}$  clearance from bass single cones ( $52 \text{ s}^{-1}$  rate) derived from fits between experimental and theoretical data is close in value to the 43 ms time constant measured from light-dependent changes in cytoplasmic free  $\text{Ca}^{2+}$  in tiger salamander cones (Sampath et al., 1999).

#### *Differences in PDE Inactivation Kinetics between Rods and Cones*

Biochemical studies have demonstrated that the catalytic efficiency of active PDE is essentially the same in rods and cones (Gillespie and Beavo, 1988; Cote et al., 2002). In contrast, we have shown here that the lifetime of the active state of PDE is  $\sim 10$  times longer in rods than in cones. This profound difference in active PDE lifetime had been anticipated as a theoretical possibility in previous models of cone phototransduction (Sneyd and Tranchina, 1989; Ichikawa, 1994; Hamer and Tyler, 1995; Korenbrot and Rebrink, 2002). A biochemical study of isolated fish rods and cones has previously suggested that the rate of PDE inactivation is faster in cones than in rods (Tachibanaki et al., 2001), but the magnitude of the rod cone differences observed in the biochemical preparation is about one third as large as we report here. At this time, the functional integrity of the biochemical preparation may be compromised and

quantitative information is likely more reliable as measured in the intact cells.

There are structural differences that can help explain the functional difference between rod and cone PDE. Photoreceptor PDE is a type 6 isoform (for review see Beavo, 1995). In cones, inactive PDE consists of two identical catalytic subunits ( $\alpha$ ) and two identical inhibitory subunits ( $\gamma_{\text{cone}}$ ) (Gillespie and Beavo, 1988; Cote et al., 2002). In rod PDE, in contrast, the inactive enzyme consists of two different catalytic subunits ( $\alpha$  and  $\beta$ ) and two inhibitory subunits,  $\gamma_{\text{rod}}$ . Importantly,  $\gamma_{\text{cone}}$  and  $\gamma_{\text{rod}}$  are unique molecules that differ in molecular weight and in their affinity to bind their respective catalytic subunits (Hamilton and Hurley, 1990; Hamilton et al., 1993). The interactions between inhibitory and catalytic subunits are not defined by the law of mass action alone, but are regulated by noncatalytic cGMP binding to a regulatory GAF domain in the catalytic subunits (for review see Cote, 2004). The molecular details of the regulatory interactions between catalytic and inhibitory subunits, cGMP, and the GAF domain are presently under study. It will not be surprising to learn that these regulatory events differ between the two photoreceptor types.

Functional difference in the interaction between catalytic and inhibitory units in PDE can help explain differences in the activation rates between rods and cones, but different mechanisms must be invoked to explain the difference in the inactivation rate. Activation follows separation of  $\gamma$  from the catalytic subunits, but the  $\gamma$  subunit cannot escape too far, otherwise it could not return as quickly as it must. This imposes either some geometrical constraints on the diffusion process of the free  $\gamma$  subunit or the  $\gamma$  subunit is really never freed in the activation process, but remains tethered to the rest of the molecule. In this context, it is noteworthy that the regulatory protein RGS-9 is 10 times more abundant in cones than in rods (Zhang et al., 2003), and its function helps control photocurrent recovery (Chen et al., 2000). Perhaps the difference in RGS9 concentration between rods and cones acts as a confinement mechanism that restricts  $\gamma$  surface diffusion and controls PDE lifetime.

#### *Photoresponse: Implications for Rod Cone Functional Differences*

The molecular events of PDE activation are better understood than those involved in its deactivation. In the analysis we report here, we have measured the rate of spontaneous, thermal activation in cones and found it to be not significantly different from that in rods. PDE activation by light involves collisions between activated (GTP-bound) transducin and PDE that cause separation of inhibitory  $\gamma$  subunits from the  $\alpha/\beta$  dimer. The limiting rate of light-dependent

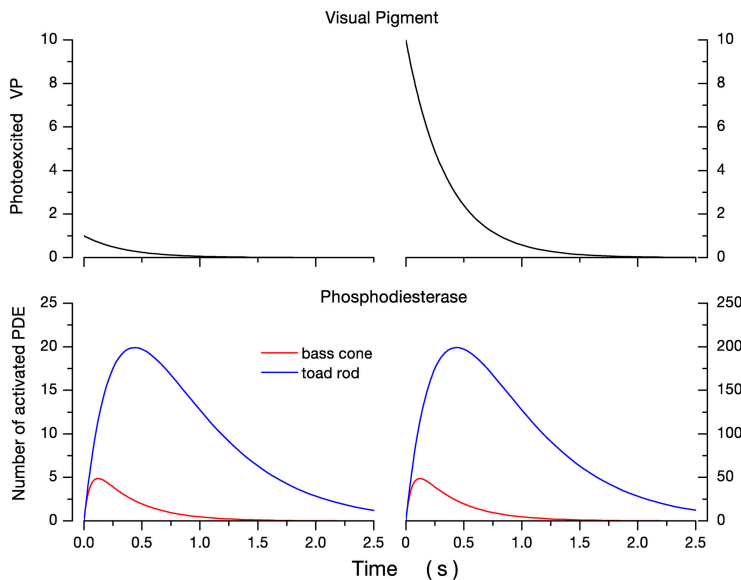
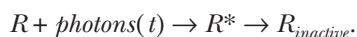


FIGURE 7. Simulations of the expected time course of photoexcited VP and PDE in nonmammalian rods and cones at room temperature. The left panels illustrate the response to a single excited VP molecule and those on the right the response to 10 molecules. Simulations are based on the lifetime of active PDE in rods and cones derived from dark noise analysis by Rieke and Baylor (1996) or this report (Table II). The lifetime of PDE is 10 times shorter in cones than in rods (54 ms and 555 ms, respectively). As a consequence, it can be expected that when the same number of visual pigment molecules are excited in the photoreceptors, the total number of activated PDE molecules will be less in cones than rods, and this number will be reached more rapidly in cones than in rods.

photocurrent activation is essentially the same in rods and cones (Hestrin and Korenbrot, 1990). The rate of thermal deactivation is faster in cones than rods. However, in both instances, the mechanism of inactivation requires the reassociation of  $\alpha/\beta$  dimers with inhibitory  $\gamma$  subunits.

To anticipate the functional consequence of the rod cone differences in PDE inactivation kinetics we report here, we computed the expected time course of PDE activation by excited VP in rods and cones based on the kinetic data we report here. We applied a simplified deterministic model based on a coupled system of differential equations previously developed by others that successfully simulates photocurrents (Forti et al., 1989; Sneyd and Tranchina, 1989; Hamer, 2000). The kinetics of excited VP, denoted by  $R^*$ , is described by the reaction



VP is excited instantaneously by light delivered with characteristic time course,  $\text{photons}(t)$ .  $R^*$  inactivates irreversibly with a rate constant  $\tau_R^{-1}$ . The dynamics of this process is described by

$$\frac{dR(t)^*}{dt} = \text{photons}(t)R - \frac{R(t)^*}{\tau_R}. \quad (1.14)$$

We assume that VP kinetics are the same in rods and cones with  $\tau_R = 0.35$  s, a value that successfully simulates rod photocurrent kinetics (Forti et al., 1989; Sneyd and Tranchina, 1989; Hamer, 2000). This is a useful assumption to illustrate the difference in PDE kinetics between rods and cones, but in reality, the excited VP lifetime may differ in rods and cones since they have distinct rhodopsin kinase, an enzyme that helps determine this lifetime. The dynamics of acti-

vated PDE molecules,  $N^*(t)$ , produced by  $R(t)^*$  are given by

$$\frac{dN^*(t)}{dt} = V_{PDE}R^*(t) - \frac{N^*(t)}{\tau}, \quad (1.15)$$

where  $V_{PDE} = N^*/R^* = 125$  per second per  $R^*$  (Leskov et al., 2000) is the mean stoichiometric rate and  $\tau$  is the lifetime of active PDE. We assume that PDE lifetime (Table II) is constant, regardless of the means of activation (whether light or heat driven). There is no a priori reason to expect this rate to be different whether PDE is recovering from thermal or transducin-dependent activation.

Simulation of the system of Eqs. 1.14–1.15 yields the results illustrated in Fig. 7. Shown are the time course of PDE activation caused by flash (instantaneous) excitation of 1 and 10 VP molecules. Since we assume the initial amplification process is similar in cones and rods (Hestrin and Korenbrot, 1990), then the initial onset of PDE activity is similar in rods and cones. However, for a given light intensity, the peak number of activated PDE molecules and the time to reach the peak is smaller and faster in cones than in rods. For example, a single excited opsin activates a maximum of five PDE molecules at a peak time of 200 ms. In rods, in contrast, 20 PDE molecules are active at the peak time of 500 ms. The simulation is valid only at dim light levels, as long as  $V_{PDE}$  remains constant.

### Conclusion

Experimental and theoretical analysis of dark current fluctuations in cones and in rods reveals a difference in the lifetime of active PDE between receptor types. As a consequence, it can be predicted that for a given number of photoexcited opsins, fewer PDE molecules will

be activated with a shorter time to peak in cones than in rods. These differences will result in a loss of cGMP that is smaller and faster in cones than rods.

The difference in PDE lifetime between rods and cones must inevitably result in (1) a photocurrent time to peak faster in cones than rods, and (2) a signal gain (cGMP hydrolyzed per second per photon) smaller in cones than rods. These functional differences are, indeed, hallmarks of the difference in the transduction signal between the receptor types. This PDE functional difference is important, but it must be understood to be but one among several molecular mechanisms that determine in detail the difference between rod and cone transduction signals and, specifically, their rates of deactivation.

## APPENDIX

### Appendix 1: Stochastic Equation To Describe PDE Activity Fluctuations

We assume PDE activation is driven by thermal fluctuation. Each activation event is independent from any other. The total number of PDE molecules in the cone outer segment,  $N_0$ , is distributed between active  $N^*(t)$  and inactive states  $N(t)$ . Transitions between inactive and active states occur with forward activation rate  $k_a$ , and backward activation rate (inactivation rate)  $\tau^{-1}$ . Because the mean number  $\langle N^*(t) \rangle$  of active PDE molecules in darkness over the entire outer segment is large ( $>10$ ), the stochastic activation kinetics is well approximated by the Ornstein-Uhlenbeck process.

The mean number  $\langle N^*(t) \rangle$  satisfies the equation

$$\frac{dN^*(t)}{dt} = k_a N(t) - \frac{N^*(t)}{\tau}, \quad (\text{A1.1})$$

where  $N(t) + N^*(t) = N_0$ . At equilibrium,

$$N^* = \frac{k_a}{k_a + \tau^{-1}} N_0. \quad (\text{A1.2})$$

The stochastic component can be derived by noting that the thermal fluctuations in the number of active PDE follows Poisson statistics, where the variance  $\sigma_0$  is given by

$$\sigma_0 = \sqrt{\frac{k_a \tau^{-1} N_0}{(k_a + \tau^{-1})^2}}. \quad (\text{A1.3})$$

An effective stochastic equation, describing the dynamics of  $N^*(t)$  is given by

$$dN^*(t) = \left( k_a N(t) - \frac{dN^*(t)}{\tau} \right) dt + \sigma_0 dw, \quad (\text{A1.4})$$

where  $dw$  is the standard white noise. We use

$$dN^*(t) = (\alpha_1 - \alpha_2 N^*(t)) dt + \sigma_0 dw, \quad (\text{A1.5})$$

where  $\alpha_1 = k_a N_0$  and  $\alpha_2 = (1/\tau + k_a)$ .

Finally, the power density spectrum  $S(\omega)$  of  $N^*$  is a Lorentzian given by

$$S(\omega) = \frac{\sigma_0^2/4}{\alpha_2^2 + \omega^2}. \quad (\text{A1.6})$$

### Appendix 2: Spectral Density of cGMP Concentration in a $\text{Ca}^{2+}$ -buffered Cone Outer Segment

To derive an equation that describes cGMP concentration, we note that cGMP molecules diffuse along the cone outer segment (Holcman and Korenbrot, 2004) and local fluctuations in concentration create local gradients. If, on average, 60 PDE molecules are active in the dark at random locations in the cone outer segment, then local diffusion is important in maintaining equilibrium between PDE and GC activity. In the analysis we present here, nonetheless, we neglect longitudinal diffusion. This is justified because in whole-cell mode, measured current noise is averaged over the entire outer segment. The electrophysiological method does, by its nature, average the effect of local diffusion. Hence, we derive an equation for the total number of cGMP by space averaging.

The averaged equation is derived as follows: at fixed calcium concentration, cGMP concentration fluctuates because of the dynamics of its synthesis by GC, its hydrolysis by PDE, and its longitudinal diffusion within the cone outer segment. These contributions are expressed in the following partial differential equation and its boundary conditions

$$\frac{\partial c(s,t)}{\partial t} = D \frac{\partial^2 c(s,t)}{\partial s^2} - k_{sub} N^*(t) c(s,t) + \gamma, \quad (\text{A2.1})$$

for  $x \in [0, L]$ ,

$$\frac{\partial}{\partial n} c(s,t) = 0 \text{ for } s = 0, L.$$

$c(s,t)$  is cGMP concentration at position  $s$  and time  $t$ ,  $D$  is the longitudinal diffusion constant, and  $L$  is outer segment length.  $\gamma$  is the GC reaction rate, which does not fluctuate when  $\text{Ca}^{2+}$  is strongly buffered.  $k_{sub} N^*(t)$  is the PDE reaction rate. Following conventional enzyme kinetics,

$$k_{sub} = \frac{k_{CAT}/2}{K_{mcGMP}},$$

where  $k_{CAT}$  is the hydrolysis turnover rate per active PDE molecule,  $K_{mcGMP}$  is the cGMP Michaelis-Menten constant of PDE, and  $N^*(t)$  is the number of active PDE molecules.  $k_{CAT}$  is divided by 2 because the active PDE enzyme is a dimer.

The number of active PDE molecules varies continuously about its mean value according to the stochastic equation (A1.4). A coarse grained equation for the

dark noise is obtained from expressions (A.1.1 and A.2.1) by spatial averaging over  $s$ . Let

$$C(t) = \frac{\int_0^L c(s,t) ds}{V_T}$$

be the concentration cGMP in the outer segment of volume  $V_p$  then

$$\frac{dN^*}{dt} = (\alpha_1 - \alpha_2 N^*) + \sigma_0 \frac{dw}{dt} \quad (\text{A2.2})$$

$$\frac{dC}{dt} = -k_{sub} N^* C + \gamma. \quad (\text{A2.3})$$

From Eqs. 1.4 and 1.5, it is possible to compute the spectrum of the noise of the linear system near the equilibrium point of the deterministic system (no noise). In general, the steady-state noise for a nonlinear system of equation can only be estimated using the Fokker-Planck equation associated with system A2.2–2.3.

Since Eqs. 1.4 and 1.5 present a unique steady-state attractor of coordinates,

$$n_0 = N_0 \frac{k_a}{\tau^{-1} + k_a}$$

$$c_0 = \frac{\gamma(\tau^{-1} + k_a)}{k_{sub} k_a N_0}.$$

The power spectrum of  $C(t)$  can be computed by linearizing the system around  $n_0, c_0$  as follows. Let us write

$$N^*(t) = n_0 + \varepsilon n_1(t) + \dots$$

$$C(t) = c_0 + \varepsilon c_1(t) + \dots$$

then at the first order,  $n_1, c_1$  are solution of

$$\frac{dn_1^*}{dt} = -\alpha_2 n_1 + \sigma_0 \dot{w} \quad (\text{A2.4})$$

$$\frac{dc_1}{dt} = -k_{sub}(c_0 n_1^* + c_1 n_0). \quad (\text{A2.5})$$

The eigenvalues of the deterministic system (A2.4–A2.5) are  $\lambda_1 = -\alpha_2$  and  $\lambda_2 = -k_{sub} c_0$ .

The power density spectrum  $S(\omega)$  is obtained by first linearizing the system and then using the Fourier transform.  $S(\omega)$  is the product of two Lorentzians  $S_1$  and  $S_2$ , of characteristic frequencies  $\omega_1$  and  $\omega_2$  defined by the kinetics of PDE activation

$$S_1(\omega) = \frac{\sigma_0^2/4}{\alpha_1^2 + \omega^2}$$

$$S_2(\omega) = \frac{(k_{sub} c_0)^2/4}{(k_{sub} n_0)^2 + \omega^2}$$

and

$$S(\omega) = S_1(\omega) S_2(\omega) = \frac{(k_{sub} c_0)^2 \sigma_0^2}{16} \frac{1}{\omega_1^2 + \omega^2} \frac{1}{\omega_2^2 + \omega^2}, \quad (\text{A2.6})$$

where  $\omega_1 = \alpha_2 = k_a + \tau^{-1}$  and  $\omega_2 = k_{sub} N_0^*$ .

The power spectrum of the current is computed from the power spectrum of cGMP fluctuations, using the known relationship between current amplitude and cGMP concentration at a fixed  $\text{Ca}^{2+}$  concentration in bass cone membranes (Rebrink et al., 2000):

$$I_m(t) = I_{max} \frac{C^n(t)}{C^n(t) + K_{cG}^n}, \quad (\text{A2.7})$$

where  $I_{max}$  is the maximum current,  $K_{cG}$  is the concentration at half maximal current, and  $n$  is a constant to denote cooperativity in channel activation. When  $C^n(t) \ll K_{cG}^n$ , the current power density spectrum  $S_I(\omega)$  is

$$S_I(\omega) = 9 c_0^4 (I_{max}/K_{cG}^n)^2 S(\omega). \quad (\text{A2.8})$$

### Appendix 3: Estimation of Dark cGMP Synthesis Rate $\gamma_{dark}$

Zaprinast is assumed to instantly and totally suppress dark PDE activity. The dark rate of cGMP synthesis,  $\gamma_{dark}$ , is estimated by measuring the linear rate of current increase at the moment zaprinast is delivered,  $t = 0$ . The method of experimental analysis is described by a reduced system of the equations ( $S_d$ ):

$$\frac{dC}{dt} = \frac{\gamma_{max}}{1 + Ca^2/K_{GC}^2}$$

$$\frac{dCa}{dt} = \Omega I(c, Ca) - \phi Ca$$

$$I(c, Ca) = A \frac{C^n}{K_c^n(Ca)}$$

$$K_c(Ca) = K_{min} + (K_{max} - K_{min}) \frac{Ca}{Ca + K_m^c},$$

where the PDE rate is set to zero in 1.11. The initial condition for cGMP and Ca concentration, are the steady-state values,  $C(0) = C_0$  and  $Ca(0) = Ca_0$ .

The value  $\gamma_m$  can be estimated from system  $S_d$  by computing the derivative of the current at time 0. This procedure avoids the need to find an analytic solution of system  $S_d$ .

The time derivative of the current is given by

$$\begin{aligned} \frac{dI}{dt} &= nA \frac{C^{n-1}}{K_c^3(Ca)} \frac{dC}{dt} - nA \frac{C^n}{K_c^{n+1}(Ca)} \frac{dK_c(Ca)}{dt} \quad (\text{A3.1}) \\ &= nA \frac{C^{n-1}}{K_c^n(Ca)} \frac{\gamma_{dark}}{1 + Ca^2/K_{GC}^2} - \\ & nA \frac{C^n}{K_c^{n+1}(Ca)} \frac{K_m^c}{(Ca + K_m^c)^2} (\Omega I(c, Ca) - \phi Ca). \end{aligned}$$

At time  $t = 0$ , using system ( $S_d$ ), we obtain that

$$\left. \frac{dI}{dt} \right|_{t=0} = nA \frac{C_0^{n-1}}{K_c^n (Ca_0) 1 + Ca_0^2 / K_{GC}^2} - nA \frac{C_0^n}{K_c^{n+1} (Ca_0) (Ca_0 + K_m)^2} (\Omega I(c, Ca_0) - \phi Ca_0)$$

$$I(c, Ca_0) = A \frac{C_0^n}{K_c^n (Ca_0)}$$

Finally,

$$\gamma_{dark} = \frac{\left. \frac{dI}{dt} \right|_{t=0} + B}{D},$$

where the quantities

$$D = nA \frac{C_0^{n-1}}{K_c^n (Ca_0) 1 + Ca_0^2 / K_{GC}^2} \frac{1}{K_c^n (Ca_0)}$$

and

$$B = nA \frac{C_0^n}{K_c^{n+1} (Ca_0) (Ca_0 + K_m)^2} (\Omega I(c, Ca_0) - \phi Ca_0)$$

are computed at time  $t = 0$ .

*Appendix 4: Spectral Density of cGMP Concentration in a Normal Cone Outer Segment. Analysis of the Dark Noise Equation ( $S_c$ )*

We derive first the steady state for system  $S_c$  and then from the linearized equation around the steady state, we derive the analytic expression of the power spectrum. Finally, we prove by computing the eigenvalues of the matrix of the linearized system that the effect of  $Ca^{2+}$  on system  $S_c$  is to reduce the extent of cGMP fluctuations.

Denoting  $\tilde{\Omega} = (I_{max} \Omega) / (K_{Ca}^{GC})$  for  $Ca^{++} \gg K_{Ca}^{GC}$ , the steady state of the deterministic part of equation  $S_c$  consists of a single attractor of coordinates  $(n_0, c_0, Ca_0)$ .

$$n_0 = \frac{k_a}{k_a + \tau^{-1}} N_0$$

$$c_0 = \left( \frac{\phi \gamma_0 (K_{Ca}^{GC})^2}{k_{sub} N_0 \tilde{\Omega}^3} \right)^{1/7}$$

$$Ca_0 = \left( \frac{\phi}{\tilde{\Omega}} \right)^{2/7} \left( \frac{\gamma_0 (K_{Ca}^{GC})^2}{k_{sub} N_0} \right)^{3/7}$$

The power spectrum can be computed by linearizing system  $S_c$  around  $(n_0, c_0, Ca_0)$ . If we expand the solutions in series,

$$N^*(t) = n_0 + \varepsilon n_1(t) + \dots \quad (A4.1)$$

$$C(t) = c_0 + \varepsilon c_1(t) + \dots \quad (A4.2)$$

$$Ca(t) = Ca_0 + \varepsilon Ca_1(t) + \dots \quad (A4.3)$$

then the linearized part of  $S_c$  is given by

$$\frac{dn_1}{dt} = -\alpha_2 n_1 + \sigma_0 \dot{w}$$

$$\frac{dc_1}{dt} = -k_{sub} n_0 c_1 - k_{sub} n_1 c_0 - 2 \frac{\gamma_0 Ca_0}{(K_{Ca}^{GC})^2 \left( 1 + \frac{Ca_0^2}{K_{Ca}^{GC}} \right)^2} Ca_1$$

$$\frac{dCa_1}{dt} = D_1 c_1 - \phi Ca_1,$$

where

$$D_1 = \Omega P f \frac{n_0^{n-1}}{(K_{GMP}(Ca))^n}.$$

Using the Fourier transform of the linearized system, after some computation, we obtain expression for the power spectrum of  $c_1$ , given by

$$S(\omega) = \frac{\sigma_0^2 / 4}{\omega^2 + \omega_1^2} \frac{(k_{sub} c_0)^2 / 4}{\left( \omega_2 + \frac{\theta \phi}{\phi^2 + \omega^2} \right)^2 + \omega^2 \left( 1 - \frac{\theta}{\phi^2 + \omega^2} \right)^2} \quad (A4.4)$$

where  $\theta = D_1 \zeta$  and

$$\zeta = \frac{2 Ca_0}{(K_{Ca}^{GC})^2 [1 + (Ca_0)^2 / (K_{Ca}^{GC})^2]^2} \frac{\gamma_{max}}{K_{Ca}^{GC}}.$$

The stability of the system  $S_c$  around the attractor  $(n_0, c_0, Ca_0)$  depends on the eigenvalues of the matrix L of the linearized system

$$L = \begin{bmatrix} -\alpha_2 & 0 & 0 \\ -k_{sub} n_0 & -k_{sub} c_0 & -\zeta \\ 0 & D_1 & -\phi \end{bmatrix}$$

The eigenvalues are

$$\lambda_1 = -\alpha_2,$$

$$\lambda_2 = \frac{-(\phi + k_{sub} c_0) - \sqrt{(\phi - k_{sub} c_0)^2 - 4D\zeta}}{2},$$

$$\lambda_3 = \frac{-(\phi + k_{sub} c_0) + \sqrt{(\phi - k_{sub} c_0)^2 - 4D\zeta}}{2}.$$

By expanding  $\lambda_2$  in terms of  $D\zeta$  and comparing with the similar eigenvalue for the calcium-buffered system, we obtain that

$$\lambda_2 = -k_{sub} c_0 - \frac{D\zeta}{\phi - k_{sub} c_0} \left( 1 - \frac{2D\zeta}{\phi - k_{sub} c_0} + o(D\zeta) \right).$$

Since  $\phi > k_{sub}c_0$ , the present expression of  $\lambda_2$  shows that the effect of calcium dynamics is to create a negative shift in the cGMP time constant. That is, calcium dynamics stabilizes the cGMP fluctuation and thus any fluctuations will relax to the steady state, much faster than in the absence of calcium dynamics.

We thank J. Schnapf, T. Rebrük, and an anonymous reviewer for valuable insight in the review of this manuscript.

D. Holcman is incumbent to the Madeleine Haas Russell Chair and gratefully acknowledges support from the Sloan-Swartz foundation. This work was supported by National Institutes of Health grant EY-05498 and The Sandler Program in Basic Sciences at UCSF.

Lawrence G. Palmer served as editor.

Submitted: 24 February 2005

Accepted: 25 April 2005

#### REFERENCES

- Barnes, S., and B. Hille. 1989. Ionic channels of the inner segment of tiger salamander cone photoreceptors. *J. Gen. Physiol.* 94:719–743.
- Baylor, D.A., T.D. Lamb, and K.W. Yau. 1979. Responses of retinal rods to single photons. *J. Physiol.* 288:613–634.
- Baylor, D.A., G. Matthews, and K.W. Yau. 1980. Two components of electrical dark noise in toad retinal rod outer segments. *J. Physiol.* 309:591–621.
- Baylor, D.A., B.J. Nunn, and J.L. Schnapf. 1984. The photocurrent, noise and spectral sensitivity of rods of the monkey macaca fascicularis. *J. Physiol.* 357:575–607.
- Beavo, J.A. 1995. Cyclic nucleotide phosphodiesterases: functional implications of multiple isoforms. *Physiol. Rev.* 75:725–748.
- Chen, C.K., M.E. Burns, W. He, T.G. Wensel, D.A. Baylor, and M.I. Simon. 2000. Slowed recovery of rod photoresponse in mice lacking the GTPase accelerating protein RGS9-1. *Nature.* 403:557–560.
- Cobbs, W.H., A.E. Barkdoll III, and E.N. Pugh Jr. 1985. Cyclic GMP increases photocurrent and light sensitivity of retinal cones. *Nature.* 317:64–66.
- Cote, R.H. 2004. Characteristics of photoreceptor PDE PDE6.: similarities and differences to PDE5. *Int. J. Impot. Res.* 16(Suppl 1): S28–S33.
- Cote, R.H., A.E. Daly, B.A. Valeriani, and N. Vardi. 2002. Regulation of cone photoreceptor phosphodiesterase PDE6C by its inhibitory subunit and by cGMP binding. Investigative Ophthalmology and Visual Science. ARVO Meetings. Abstract 1960.
- D'Amours, M.R., and R.H. Cote. 1999. Regulation of phosphodiesterase catalysis by its non-catalytic cGMP-binding sites. *Biochem. J.* 340:863–869.
- Dumke, C.L., V.Y. Arshavsky, P.D. Calvert, M.D. Bownds, and E.N. Pugh Jr. 1994. Rod outer segment structure influences the apparent kinetic parameters of cyclic GMP phosphodiesterase. *J. Gen. Physiol.* 103:1071–1098.
- Donner, K., S. Hemila, and A. Koskelainen. 1998. Light adaptation of cone photoresponses studied at the photoreceptor and ganglion cell levels in the frog retina. *Vision Res.* 38:19–36.
- Ebrey, T., and Y. Koutalos. 2001. Vertebrate photoreceptors. *Prog. Retin. Eye Res.* 20:49–94.
- Forti, S., A. Menini, G. Rispoli, and V. Torre. 1989. Kinetics of phototransduction in retinal rods of the newt *Triturus cristatus*. *J. Physiol.* 419:265–295.
- Gillespie, P.G., and J.A. Beavo. 1988. Characterization of a bovine cone photoreceptor phosphodiesterase purified by cyclic GMP-sepharose chromatography. *J. Biol. Chem.* 263:8133–8141.
- Gillespie, P.G., and J.A. Beavo. 1989. Inhibition and stimulation of photoreceptors phosphodiesterase by dipyrindamole and M&B 22,948. *Mol. Pharmacol.* 36:773–781.
- Gorczyca, W.A., A.S. Polans, I.G. Surgucheva, I. Subbaraya, W. Baehr, and K. Palczewski. 1995. Guanylyl cyclase activating protein. A calcium-sensitive regulator of phototransduction. *J. Biol. Chem.* 270:22029–22036.
- Hackos, D.H., and J.I. Korenbrot. 1999. Divalent cation selectivity is a function of gating in native and recombinant cyclic nucleotide-gated ion channels from retinal photoreceptors. *J. Gen. Physiol.* 113:799–818.
- Hamer, R.D. 2000. Computational analysis of vertebrate phototransduction: combined quantitative and qualitative modeling of dark- and light-adapted responses in amphibian rods. *Vis. Neurosci.* 17:679–699.
- Hamer, R.D., and C.W. Tyler. 1995. Phototransduction: modeling the primate cone flash response. *Vis. Neurosci.* 12:1063–1082.
- Hamilton, S.E., and J.B. Hurley. 1990. A phosphodiesterase inhibitor specific to a subset of bovine retinal cones. *J. Biol. Chem.* 265: 11259–11264.
- Hamilton, S.E., R.K. Prusti, J.K. Bentley, J.A. Beavo, and J.B. Hurley. 1993. Affinities of bovine photoreceptor cGMP phosphodiesterases for rod and cone inhibitory subunits. *FEBS Lett.* 318: 157–161.
- Harosi, F.I. 1976. Spectral relations of cone pigments in goldfish. *J. Gen. Physiol.* 68:65–80.
- Hestrin, S., and J.I. Korenbrot. 1990. Activation kinetics of retinal cones and rods: response to intense flashes of light. *J. Neurosci.* 10:1967–1973.
- Hodgkin, A.L., and B.J. Nunn. 1988. Control of light-sensitive current in salamander rods. *J. Physiol.* 403:439–471.
- Holcman, D., and J.I. Korenbrot. 2004. Longitudinal diffusion in retinal rod and cone outer segment cytoplasm: the consequence of cell structure. *Biophys. J.* 86:2566–2582.
- Ichikawa, K. 1994. Transduction steps which characterize retinal cone current responses to flash stimuli. *Neurosci. Res.* 20:337–343.
- Johnson, R.L., K.B. Grant, T.C. Zankel, M.F. Boehm, S.L. Merbs, J. Nathans, and K. Nakanishi. 1993. Cloning and expression of goldfish opsin sequences. *Biochemistry.* 32:208–214.
- Jones, G.J., M.C. Cornwall, and G.L. Fain. 1996. Equivalence of background and bleaching desensitization in isolated rod photoreceptors of the larval tiger salamander. *J. Gen. Physiol.* 108:333–340.
- Kawamura, S., and S. Yokoyama. 1998. Functional characterization of visual and nonvisual pigments of American chameleon *Anolis carolinensis*. *Vision Res.* 38:37–44.
- Kefalov, V., Y. Fu, N. Marsh-Armstrong, and K.W. Yau. 2003. Role of visual pigment properties in rod and cone phototransduction. *Nature.* 425:526–531.
- Koch, K.W., and L. Stryer. 1988. Highly cooperative feedback control of retinal rod guanylate cyclase by calcium ions. *Nature.* 334: 64–66.
- Korenbrot, J.I. 1995. Ca<sup>2+</sup> flux in retinal rod and cone outer segments: differences in Ca<sup>2+</sup> selectivity of the cGMP-gated ion channels and Ca<sup>2+</sup> clearance rates. *Cell Calcium.* 18:285–300.
- Korenbrot, J.I., and T.I. Rebrük. 2002. Tuning outer segment Ca<sup>2+</sup> homeostasis to phototransduction in rods and cones. *Adv. Exp. Med. Biol.* 514:179–203.
- Lamb, T.D., and E.J. Simon. 1977. Analysis of electrical noise in turtle cones. *J. Physiol.* 272:435–468.
- Leibrock, C.S., and T.D. Lamb. 1997. Effect of hydroxylamine on photon-like events during dark adaptation in toad rod photoreceptors. *J. Physiol.* 501:97–109.

- Leskov, I.B., V.A. Klenchin, J.W. Handy, G.G. Whitlock, V.I. Govardovskii, M.D. Bownds, T.D. Lamb, E.N. Pugh Jr., and V.Y. Arshavsky. 2000. The gain of rod phototransduction: reconciliation of biochemical and electrophysiological measurements. *Neuron*. 27:525–537.
- Maricq, A.V., and J.I. Korenbrot. 1990a. Inward rectification in the inner segment of single retinal cone photoreceptors. *J. Neurophysiol.* 64:1917–1928.
- Maricq, A.V., and J.I. Korenbrot. 1990b. Potassium currents in the inner segment of single retinal cone photoreceptors. *J. Neurophysiol.* 64:1929–1940.
- Matthews, H.R., G.L. Fain, R.L. Murphy, and T.D. Lamb. 1990. Light adaptation in cone photoreceptors of the salamander: a role for cytoplasmic calcium. *J. Physiol.* 420:447–469.
- Miller, D.L., and J.I. Korenbrot. 1987. Kinetics of light-dependent Ca fluxes across the plasma membrane of rod outer segments. A dynamic model of the regulation of the cytoplasmic Ca concentration. *J. Gen. Physiol.* 90:397–425.
- Miller, J.L., and J.I. Korenbrot. 1993. Phototransduction and adaptation in rods, single cones, and twin cones of the striped bass retina: a comparative study. *Vis. Neurosci.* 10:653–667.
- Nakatani, K., and K.W. Yau. 1988. Calcium and light adaptation in retinal rods and cones. *Nature*. 334:69–71.
- Nikonov, S., T.D. Lamb, and E.N. Pugh Jr. 2000. The role of steady phosphodiesterase activity in the kinetics and sensitivity of the light-adapted salamander rod photoresponse. *J. Gen. Physiol.* 116:795–824.
- Ohyama, T., D.H. Hackos, S. Frings, V. Hagen, U.B. Kaupp, and J.I. Korenbrot. 2000. Fraction of the dark current carried by Ca<sup>2+</sup> through cGMP-gated ion channels of intact rod and cone photoreceptors. *J. Gen. Physiol.* 116:735–754.
- Pepperberg, D.R., and T.I. Okajima. 1992. Hydroxylamine-dependent inhibition of rhodopsin phosphorylation in the isolated retina. *Exp. Eye Res.* 54:369–376.
- Perry, R.J., and P.A. McNaughton. 1991. Response properties of cones from the retina of the tiger salamander. *J. Physiol.* 433:561–587.
- Picones, A., and J.I. Korenbrot. 1994. Analysis of fluctuations in the cGMP-dependent currents of cone photoreceptor outer segments. *Biophys. J.* 66:360–365.
- Pugh, E.N., Jr., and T.D. Lamb. 2000. Phototransduction in vertebrate rods and cones: molecular mechanisms of amplification, recovery and light adaptation. In *Handbook of Biological Physics*. Volume 3. D.G. Stavenga, W.J. DegRip, and E.N. Pugh Jr., editors. Elsevier Science Publishing Co. Inc., Amsterdam. 186–255.
- Rebrik, T.I., and J.I. Korenbrot. 1998. In intact cone photoreceptors, a Ca<sup>2+</sup>-dependent, diffusible factor modulates the cGMP-gated ion channels differently than in rods. *J. Gen. Physiol.* 112:537–548.
- Rebrik, T.I., E.A. Kotelnikova, and J.I. Korenbrot. 2000. Time course and Ca<sup>2+</sup> dependence of sensitivity modulation in cyclic GMP-gated currents of intact cone photoreceptors. *J. Gen. Physiol.* 116:521–534.
- Rieke, F., and D.A. Baylor. 1996. Molecular origin of continuous dark noise in rod photoreceptors. *Biophys. J.* 71:2553–2572.
- Rieke, F., and D.A. Baylor. 2000. Origin and functional impact of dark noise in retinal cones. *Neuron*. 26:181–186.
- Sampath, A.P., and D.A. Baylor. 2002. Molecular mechanism of spontaneous pigment activation in retinal cones. *Biophys. J.* 83:184–193.
- Sampath, A.P., H.R. Matthews, M.C. Cornwall, J. Bandarchi, and G.L. Fain. 1999. Light-dependent changes in outer segment free-Ca<sup>2+</sup> concentration in salamander cone photoreceptors. *J. Gen. Physiol.* 113:267–277.
- Schnapf, J.L., B.J. Nunn, M. Meister, and D.A. Baylor. 1990. Visual transduction in cones of the monkey macaca fascicularis. *J. Physiol.* 427:681–713.
- Schneeweis, D.M., and J.L. Schnapf. 1999. The photovoltage of macaque cone photoreceptors: adaptation, noise, and kinetics. *J. Neurosci.* 19:1203–1216.
- Sneyd, J., and D. Tranchina. 1989. Phototransduction in cones: an inverse problem in enzyme kinetics. *Bull. Math. Biol.* 51:749–784.
- Tachibanaki, S., S. Tsushima, and S. Kawamura. 2001. Low amplification and fast visual pigment phosphorylation as mechanisms characterizing cone photoresponses. *Proc. Natl. Acad. Sci. USA*. 98:14044–14049.
- Vu, T.Q., S.T. McCarthy, and W.G. Owen. 1997. Linear transduction of natural stimuli by dark-adapted and light-adapted rods of the salamander, *Ambystoma tigrinum*. *J. Physiol.* 505:193–204.
- Wei, J.Y., E.D. Cohen, H.G. Genieser, and C.J. Barnstable. 1998. Substituted cGMP analogs can act as selective agonists of the rod photoreceptor cGMP-gated cation channel. *J. Mol. Neurosci.* 10:53–64.
- Yau, K.W., G. Matthews, and D.A. Baylor. 1979. Thermal activation of the visual transduction mechanism in retinal rods. *Nature*. 279:806–807.
- Yau, K.W., and K. Nakatani. 1985. Light-induced reduction of cytoplasmic free calcium in retinal rod outer segment. *Nature*. 313:579–582.
- Yokoyama, S. 1994. Gene duplications and evolution of the short wavelength-sensitive visual pigments in vertebrates. *Mol. Biol. Evol.* 11:32–39.
- Zhang, X., T.G. Wensel, and T.W. Kraft. 2003. GTPase regulators and photoresponses in cones of the eastern chipmunk. *J. Neurosci.* 23:1287–1297.